S1. MOVES, SPECIATE, and other emission model details

MOVES3 is used to estimate emissions and fuel use from onroad vehicle and nonroad equipment. MOVES3 includes nonroad mobile equipment within twelve sectors: recreational, construction, industrial, lawn/garden, agriculture, commercial, logging, airport support, underground mining, oil fields, pleasure craft, and railroads (railroad support equipment). MOVES3 does not include emissions from aircraft, railroad locomotives, and commercial marine vessels which are handled by the models discussed below. We used MOVES3 to estimate emissions for all nonroad sectors, except airport ground support, which are estimated using AEDT discussed below. Airport ground support only consist of 0.024% of the total NMOG emissions estimated by nonroad equipment from MOVES3 in calendar year 2016.

Within MOVES3, the estimation of emission rates and speciation is more detailed for onroad vehicles than for nonroad equipment. For onroad vehicles, MOVES stores emission rates and energy rates by detailed operating modes and emission processes. For example, MOVES classifies tailpipe exhaust emission rates into start and hot-running processes, which are further defined into operating modes. Start operating modes account for varying durations of time from when the vehicle was last started, and running operating modes are defined by acceleration, vehicle speed, and power (U.S. Epa, 2021b). To calculate emissions, MOVES requires detailed activity information (either default or user supplied), to calculate the total time corresponding to each emission process and operating mode. In addition, many of the emission rates (but not energy rates) are also stored by vehicle age to account for enhanced emission rates due to vehicle deterioration. MOVES also applies adjustment factors to emissions to account for differences in fuel properties, inspection & maintenance programs, temperature, humidity, and air conditioning usage (U.S. Epa, 2021b).

The nonroad module of MOVES estimates emission and fuel rates using more simplified methodology and data than the onroad module. For example, exhaust emissions and fuel rates for different equipment types are stored in the MOVES database as work-specific rates and are not differentiated between start and hot-running processes or individual operating modes. The MOVES nonroad module estimates exhaust emissions by multiplying the work-based emission rates by horsepower of the equipment, the number of equipment, the average hours spent in operation, and the average load of the nonroad equipment. Nonroad evaporative emissions are estimated but using simpler methodology than that used for onroad vehicles. Nonroad construction emission rates do not vary by age, and fuel-effect and temperature adjustments are limited compared to those in the onroad vehicle module (U.S. Epa, 2021b).

MOVES3 also estimates speciation with more detail for onroad vehicles than nonroad vehicles. For example, the fraction of six gaseous species from the total volatile organic compound (VOC) emissions (acetaldehyde, formaldehyde, acrolein, ethanol, benzene and 1,3-butadiene) are not estimated from SPECIATE profiles but are calculated as a function of local fuel properties (U.S. Epa, 2020a). MOVES estimates AE6 $PM_{2.5}$ species such as elemental carbon, organic carbon (OC), non-carbon organic matter (NCOM), sulfate, nitrate, ammonium and metal species, by applying SPECIATE profile fractions. The OC and NCOM fractions added to yield total OM emissions. MOVES adjusts the $PM_{2.5}$ speciation in some instances. For crankcase emissions, MOVES adjust the $PM_{2.5}$ speciation from the tailpipe exhaust speciation. Additionally, the sulfate fraction of $PM_{2.5}$ in MOVES varies with the local sulfur level of the fuel (U.S. Epa, 2020b). Thus,

the fraction of $PM_{2.5}$ species, including OM shown in Table S1a, can be different than the OM fraction for the accompanying SPECIATE profile assigned to the source.

The speciation of nonroad gaseous species is calculated using SPECIATE profile fractions within MOVES3. There are no fuel property adjustments that change the speciation like for onroad vehicles. MOVES3 does not produce speciated $PM_{2.5}$ emissions for nonroad equipment. The calculation of AE6 $PM_{2.5}$ species for nonroad is conducted outside of MOVES3 by applying SPECIATE $PM_{2.5}$ speciation profiles to the corresponding $PM_{2.5}$ nonroad emissions (U.S. Epa, 2018). Some of the speciation profiles for both gaseous and particulate matter species are derived from onroad vehicles due to more limited nonroad emissions measurements (U.S. Epa, 2018).

For MOVES-onroad, we aggregated the emissions to 22 different sources (see Table S-2; 1 to 15 are tailpipe exhaust sources, and 40 through 45 are evaporative process sources). The sources are classified as groups of vehicles that have the same VOC and PM SPECIATE Profile, which are classified by fuel type, model year, emission process, and regulatory class (vehicle technology). Different sources within the same speciation profile are divided when they have significantly different emission rates, and they constitute an important contribution of emissions when separated. For example, Source 2 (Tier 2 E10 Exhaust; Gasoline 2001-2003; Cold Start) and Source 3 (Tier 2 E10 Exhaust; Gasoline 2004+; Cold Start) use the same speciation profiles, however we identified them as different sources, because source 3 has NMOG and OM emission rates that are lower than Source 2 by approximately 50% and 30%, respectively. In addition, in 2016, Source 2 still consists of an important contribution to NMOG and OM emissions.

We similarly aggregated the emissions from nonroad to 19 sources (Table S-2) identified with unique speciation profile assignments and distinct emission rates and emission contributions. Nonroad assigns VOC SPECIATE profiles by fuel type, engine technology (2-stroke or 4-stroke), emission process, engine standard (Tier level), and aftertreatment (diesel particulate filter). In total we chose thirteen different nonroad exhaust (16 through 28), and 6 different evaporative sources (46 through 51).

The 2017 NEI marine emissions depend on vessel power, emission factors assigned to each engine and activity based on signals from Automated Identification System (AIS) transmitters. The calculation of power and the specific emission factors used are described in detail elsewhere (U.S. Epa, 2021a). AIS is a tracking system used by vessels to enhance navigation and avoid collision with other AIS transmitting vessels. The USEPA Office of Transportation and Air Quality received AIS data from the U.S. Coast Guard (USCG) to quantify all ship activity which occurred between January 1 and December 31, 2017. The provided AIS data extends beyond 200 nautical miles from the U.S. coast (Fig. S26). This boundary is roughly equivalent to the border of the U.S Exclusive Economic Zone and the North American ECA, although some non-ECA activity are captured as well. The AIS data were coupled with ship registry data that contained engine parameters, vessel power parameters, and other factors such as tonnage and year of manufacture which helped to separate the C3 vessels from the C1C2 vessels. We classified the CMV into two sources classified by the fuel-used (diesel or residual marine). We have different PM speciation profiles for diesel and residual marine, but only one profile for VOC. We recommend that future work develop specific VOC profiles for diesel and residual marine. In addition, residual marine fuel is in transition with lower sulfur content and should be updated with more recent data.

The 2017 rail inventory was developed for the 2017 NEI by the Lake Michigan Air Directors Consortium (LADCO) and the State of Illinois with support from various other states. Class I railroad emissions are based on confidential link-level line-haul activity GIS data layer maintained by the Federal Railroad Administration (FRA). In addition, the Association of American Railroads (AAR) provided national emission tier fleet mix information. Class II and III railroad emissions are based on a comprehensive nationwide GIS database of locations where short line and regional railroads operate. Passenger rail (Amtrak) emissions follow a similar procedure as Class II and III, except using a database of Amtrak rail lines. Yard locomotive emissions are based on a combination of yard data provided by individual rail companies, and by using Google Earth and other tools to identify rail yard locations for rail companies which did not provide yard data. Information on specific yards were combined with fuel use data and emission factors to create an emissions inventory for rail yards. We divided the locomotives into five sources, each of which use the same VOC and PM SPECIATE profiles.

Aircraft and aircraft ground support emissions are based primarily on the Federal Aviation Administration's (FAA) Aviation Environmental Design Tool (AEDT) (National Emissions Inventory Collaborative, 2019). The sources are divided into two sources for airport ground support (gasoline and diesel), and two for aircraft (aviation gasoline and jet fuel). Aviation gasoline is a leaded fuel that is used in piston engine aircraft. Due to limited speciation aircraft, we use the VOC and PM speciation profiles estimated from jet-fueled aircraft to the av gas fueled- aircraft. We recommend work be conducted to develop and incorporate speciation profiles from aviation gas-fueled aircraft.

SPECIATE is the U.S. EPA's repository of total organic gas and particulate matter speciation profiles of air pollution sources. Profiles within SPECIATE are paired with process-level sources in the National Emissions Inventory and other inventories developed by the Agency to speciate and/or modulate inventoried pollutants (i.e., VOC and PM25-PRI) into compound-specific species or aerosols (e.g., ethanol, acetone, elemental carbon, organic carbon). As speciation profiles generally include more species than a photochemical modeling chemical mechanism, additional post-processing on SPECIATE profiles is needed. Post-processing within the Speciation Tool translates the compound-specific species within a SPECIATE profile into the species utilized within a chemical mechanism (e.g., for Carbon Bond 6, ethanol is mapped to 1 ETOH and n-decane is mapped to 10 PAR). The output from the Speciation Tool (i.e., a GSPRO file), process-level emissions from an emissions model (e.g., MOVES), and the process-level mapping to SPECIATE profiles (i.e., a GSREF file) is then utilized by the SMOKE-MOVES emissions processing tool to generate model ready emissions for a photochemical model, such as CMAQ.

S1a. Calculation of Start-mode Emission Rates

MOVES3 start emissions are defined as "the instantaneous exhaust emissions occuring at the engine start (e.g., due to the fuel rich conditions in the cylinder to initiate combustion) as well as the additional running exhaust emissions that occur because the engine and emission control systems have not yet stabilized at the running operating temperature. Operationally, start emissions are defined as the difference in emissions between an exhaust emissions test with an ambient temperature start and the same test with the engine and emission control systems already at operating temperature." (U.S. Epa, 2021b) The annual emissions and fuel use for the start processes shown in Table S1a are consistent with this MOVES start definition

As discussed in Section S6, we use the organic matter (OM) fuel-based emission factor (mg/kg-fuel) to calculate the CROC/OM adjustment factors. In this approach, we are interested in the OM concentration in the exhaust, rather than the incremental increase in exhaust emissions due to the start. To estimate the average tailpipe emission rates when start emissions are emitted, we estimated start exhaust emission rates for Phase 1 of the LA-92 driving cycle (also referred to as the Unified Cycle), which include both MOVES start and running emissions.

The LA-92 was used in the light-duty tests conducted by May et al. (2014), used by Lu et al. (2018) to derive volatility-resolved speciation profiles. In addition, the LA-92 drive cycle, is one of the primary driving cycles used to estimate particulate matter start emissions in MOVES from light-duty vehicles (Fulper et al., 2010; U.S. Epa, 2020c).

We calculated the Phase 1 start from the MOVES inventory output by first calculating the average start emission rates, the average running emission rate per mile, the average start fuel rate, and average running fuel rate. Crankcase start and crankcase running emissions are included in these values. Then we calculated the fuel-based Phase 1 start emissions using Equation S0, which multiplies the running emission rates by 1.2 miles (which is the length of Phase 1 of the LA-92):

$$Phase\ 1\ Start\ {}^{g}/_{kg} = \frac{\left(MOVES\ start\ emission\ rate\left(\frac{g}{start}\right) + Running\ emission\ rate\left(\frac{g}{mile}\right) \times 1.2\ miles\right)}{\left(MOVES\ start\ fuel\ rate\left(\frac{kg}{start}\right) + Running\ fuel\ rate\left(\frac{kg}{mile}\right) \times 1.2\ miles\right)} \qquad \text{(S0)}$$

The Start Phase 1 emission rates are displayed in Table S1b for the five start processes NMOG, VOC, PM2.5, and OC for the five sources that include start emissions.

The Phase 1 start emission rate is also reported in Table S1a, although it is inconsistent with the start emissions and fuel emissions in Table S1a, which only include the MOVES-defined start emission and fuel usage. The Phase 1 start OM g/kg-fuel emission rates are used to determine the CROC/OM factors as discussed in Section S6. For heavy-duty diesel 2007-2009, and 2010+, the start and running emissions are already combined, so we did not calculate Phase 1 start emission rates.

S1b. Calculation of Air, Marine, and Rail Emission Rates

Representative VOC and $PM_{2.5}$ fuel-based emission factors for several sources were derived using recent literature and model runs.

No fuel estimates from airport ground-support equipment were available in the 2016v1 platform data, from which we could estimate fuel-based emission factors. We estimated fuel-based emission factors for the airport ground support using the nonroad model in MOVES3. We assigned speciation profiles to the airport ground support equipment by fuel type, emission standard level , engine technology (2-stroke or 4-stroke), emission process (e.g. exhaust or evaporative), and aftertreatment technology (DPF) as shown in Table S1c. We then calculated an average emission rate for gasoline and diesel airport support equipment. MOVES3 estimates emissions from LPG-fueled airport ground support vehicles, that are not included in the AEDT ground support inventory. This is not a critical component of aircraft support equipment. As shown in Table S1c, LPG only consist 1.2% of the NMOG emissions from all airport ground support equipment estimated from MOVES3 in 2016. The emission rate for airport ground support equipment estimated in MOVES is based on a composite of multiple SPECIATE profiles. However, in the

final results, we apply only one VOC and one PM profile to the emissions from the gasoline and diesel sources of airport ground support as shown in Table 1. Aircraft emissions were informed by Presto et al.(Presto et al., 2011) which documented measurements of a gas-turbine engine at four different engine loads. The OM emission factor was adopted directly from the average of the results of the four tests for artifact-corrected POA. Elemental carbon was also adopted from these results. The $PM_{2.5}$ emission factor was then calculated using the speciation profile applicable to aircraft (8873). Presto et al.(Presto et al., 2011) do not report as much unspeciated 'other' $PM_{2.5}$ as is present in the profile. The VOC emission factor was estimated from the 4% and 85% engine load tests.

Various locomotive emissions were summarized by Harrell and Janssen (2017) who developed an inventory for the U.S. coordinated by the Eastern Regional Technical Advisory Committee (ERTAC). The inventory report estimated annual emissions and fuel use for Class I, II, and III line-haul units and switchers. Commuter and passenger rail emissions were reported in an EPA Technical Highlight (U.S. Epa, 2009) along with future projections of emission factors in g/gal. We use the value predicted for 2016 along with an assumed rail diesel fuel density of 3.22 kg/gal. An existing PM speciation profile (SPECIATE profile number 8994) (EC/PM = 46%, was assigned to the PM emissions from the locomotives because it had similar PM composition (EC/PM ~ 50%) on two locomotives sampled over a locomotive cycle study (Mcdonald et al., 2009).

Marine representative emissions for residual fuel oil are gathered from Huang et al. (2018) who reported larger $PM_{2.5}$ emission factors than those for total hydrocarbon after sampling a vessel at sea under a wide range of engine loads and operating conditions. The low-sulfur fuel speciated emission factors from Huang et al. (2018) were most consistent with the existing speciation profile applied for marine residual fuel oil emissions. OM emission factors were 75.5% of the total $PM_{2.5}$ emissions. Elemental carbon emissions were 470 mg kg^{-1}, only 13% of the total emissions. Corbin et al. (2018) tested diesel and marine fuel oil in a variety of engine loads and found $PM_{2.5}$ emission factors to be about 900 mg kg^{-1} with 850 mg kg^{-1} attributed to OM.

Total annual fuel use for air, marine, and rail emissions were calculated as the quotient of total emissions estimated by MOVES3 and the other emission models and inventories discussed in Section S1.

S1c. Updates to VOC speciation

The liquid diesel VOC speciation profile (SPECIATE profile number 95120) estimated from Gentner et al. (2012) is applied to emissions of liquid diesel spilled during refueling. SPECIATE profile number 95120 includes a small fraction of explicit species with the remaining 83% of the mass classified as unknown. Gentner et al. (2012) characterized over 90% of the liquid diesel using lumped species characterized by functional class (Aromatics, Straight Alkanes, Branched Alkanes, Cycloalkanes, and PAHs) and by volatility bins (log10 of the saturation concentration, C*). We created a new liquid diesel speciation profile from Gentner et al. (2012) (SPECIATE profile number 95120a) that utilizes the lumped ROC species (e.g. ROCP4ARO, Single-Ring Aromatics, $C^* = 10^4$ ug m^{-3}) and the explicit species previously included in profile 95120. We assigned each explicit species to five functional groups and volatility bins. We subtracted the explicit species from the corresponding lumped species to avoid double counting the mass from the explicit

species, as illustrated in Fig. S17. The updated profile 95120a only has 5.6% mass classified as unknown.

S2. Minor corrections to mobile PM speciation

In a few cases, minor inconsistencies were discovered between the particulate matter profiles used in SPECIATE database and the data referenced by the mobile models. Profile 95219, used for onroad compressed natural gas vehicles without oxidation catalysts, was found to have incorrect fractional contributions for elemental and organic carbon in SPECIATE, but was correct in the MOVES3 input data table.

Although a minor emissions source, the OM emission rate for CNG – no aftertreatment (Source 12) calculated from MOVES3 output was unreasonably large (201 mg/kg). In contrast, the OM emission rate from the non-aftertreatment CNG transit bus from Ayala et al. (2003), used to develop SPECIATE Profile 95219, CNG – no aftertreatment was derived, was only 17 mg/kg. We updated the OM emission rate in Table S1a using 17 mg/kg. We also reduced the total PM2.5 emissions for the other species by multiplying each PM2.5 component by a factor of 0.084, calculated by dividing the updated rates by the old rate 17/201). We recommend that MOVES3 consider re-revaluating the $PM_{2.5}$ emissions rate for pre-aftertreatment CNG vehicles in future versions.

MOVES3 reported the EC/PM fraction for pre-2007 heavy-duty diesel idle (Source 7) as 21%, which is significantly lower than the EC/PM fraction in the PM profile 8995 (46%). Some of the lower EC/PM fraction is due to the inclusion of idle crankcase emissions into Source 7, which has a lower EC/PM fraction. However, the major reason for the lower EC/PM is that MOVES3 extended idle rates were unchanged from MOVES2014, although they were intended to be updated to be consistent with the Profile 8995 in MOVES3 (U.S. Epa, 2020d). We have maintained the current MOVES3 PM2.5 extended idle emissions (including PM speciation) in this analysis and recommend that the next version of MOVES be updated to be made consistent with technical documentation and SPECIATE Profile 8995.

Due to limited speciation data from nonroad sources, in the previous emission platforms, nonroad diesel emissions without diesel particulate filter aftertreatment (CI Tier 0, CI Tier 1, CI Tier 2, CI Tier 3, CI Tier 4 – No DPF, and Locomotive sources) were speciated using Profile 91106 HDDV Exhaust – Composite which is an onroad heavy-duty diesel $PM_{2.5}$ profile heavily dominated by elemental carbon (EC) emissions (77%). Two studies that sampled elemental carbon fraction from nonroad engines reported significantly lower $PM_{2.5}$ fraction of EC emissions. Gordon et al. (2013) reported EC/PM fraction of ~ 25% from a nonroad diesel engine used in a refrigeration unit. Jathar et al. (2017) reported black carbon (BC)/PM fractions of ~50% at idle and ~ 60% at 50% load for a nonroad John Deere engine without aftertreatment. Based on the lower elemental carbon fraction observed in these nonroad sources, the $PM_{2.5}$ profiles assigned to these nonroad sources were updated to use onroad Profile 8994 – Conventional Heavy-Duty Diesel Exhaust – Idle, pre-2007, which has an elemental carbon fraction of 46% which is more comparable with the reviewed non-road studies.

Profile 8873 for aircraft turbine engines was missing non-carbon organic matter and other $PM_{2.5}$. This has been updated in both SPECIATE and the speciation methods applied to output from the aircraft emissions model.

S3. NMOG sampling and characterization

Bulk total hydrocarbon (THC) emissions are typically measured with Flame-Ionization Detection (FID) (U.S. Epa, 2022) as shown in Fig. S2. In parallel, emissions are collected in Tedlar bags or canisters and analyzed with standard approaches including gas chromatography coupled with FID (GC-FID) or mass spectrometry (GC-MS). Methane is characterized with this approach and subtracted from THC to yield non-methane hydrocarbons (NMHC). Because FID methods are imprecise for characterizing carbonyls, these oxygenated compounds (e.g. formaldehyde, acetaldehyde, acrolein, etc.) are typically estimated by collecting emissions on 2,4-dinitrophenylhydrazine (DNPH) cartridges and analyzing with high-performance liquid chromatography (US EPA, 2006). Adding NMHC and carbonyl emissions yields non-methane organic gas (NMOG). While THC and methane can be measured continuously online with these methods, speciating carbonyls is performed offline over the entire emissions cycle, or major portions of it. Thus, total NMOG measurements are likewise typically provided as batch values, which limits their utility. More recently, US EPA promulgated a method for FTIR (Fourier-Transform Infrared Spectroscopy) analysis of organic gases, which could be performed online and provide continuous NMOG data. Gierczak et al. (2017) showed that FTIR methods can estimate NMOG within 5% of standard bulk methods while providing highly valuable time-resolved data with speciation of major compounds.

NMOG speciation is based on the results of the aforementioned GC-FID and GC-MS analyses. The mobile-relevant profiles stored in the SPECIATE database include between 50 and 200 compounds, depending on the source type and fuel. Often, unspeciated mass is also provided, and is reflective of the unresolved complex mixture of compounds which are either too complex to be adequately identified, or do not elute effectively from the GC column. This mass might also account, to some unknown degree, for IVOC and SVOC mass that was sorbed to the walls of the sampling bag or canister or lost to the transfer tubes, leading to a discrepancy with the bulk FID measurement. When applying speciation profiles, it is important to know what quantity the reported compound-level contributions were normalized to (e.g. NMOG, total speciated NMOG, THC, etc.). Profiles in the SPECIATE database are assumed to be normalized to total organic gas (TOG), and provide a TOG-to-regulatory-VOC factor to translate NEI VOC (National Emission Inventory Volatile Organic Carbon) emissions to a total that includes exempted species like methane and ethane. This study utilizes VOC profiles provided by Lu et al. (2018) which normalize compound contributions to the total measured emissions of compounds with vapor pressures fitting the volatility basis set definition of VOC (i.e. saturation concentration, C^*, greater than 3.2×10^6 μg m^{-3}). When considering the disparate sources across the mobile sector, it is unclear to what extent IVOCs may contribute to NMOG or TOG, although fuel properties and operating modes have critical impacts. Gasoline-fueled sources appear to have minor contributions from IVOCs (5-19%) depending on the phase of the engine test (Zhao et al., 2016), whereas diesel vehicles emit more than half of NMOG carbon as IVOCs (Zhao et al., 2015). By transitioning to a convention where vapor emissions are normalized to total Gaseous Reactive Organic Carbon (GROC), which includes both IVOCs and VOCs excluding methane, we provide a definitive and reproducible standard that will ensure consistency across source tests and experimental laboratories.

S4. GROC profiles

This section documents the algorithm and assumptions applied to create new speciation profiles for Gaseous Reactive Organic Carbon (GROC). There are several critical assumptions that must be documented. First, the GROC/NMOG ratio must be set so that NEI gaseous carbon can be translated to the GROC standard. Second, we must set the IVOC/GROC ratio. Third, we must determine a speciation profile to begin with, which will be dominated by VOC species. Fourth, we must define the IVOC speciation.

By definition, GROC includes all organic compounds in either phase with C^* greater than 320 μg m^{-3}. This excludes semivolatile organic compounds (SVOCs) and low volatility organic compounds (LVOCs), etc. According to Lu et al. (2018), the FID approach for measuring bulk NMOG yields estimates that are generally consistent with those from more comprehensive methods involving sorbent tube sampling and GC-MS analysis. One important exception was found for newer heavy-duty diesel vehicles, where the sum of carbon using the comprehensive approach exceeded the standard approach by roughly an order of magnitude. For simplicity and consistency with existing methods, we assume for now that GROC/NMOG equals unity for all sources. However, we stress that this parameter should be better constrained in the future, either with coincident bulk NMOG and GROC measurements, or with newer FTIR methods.

The IVOC/GROC ratio varies substantially depending on source type, fuel, and operating mode. Selected ratios for each exhaust source and references for each data point are given in Table S2. As future speciation profiles are published that contain quantification of explicit and lumped IVOCs as fractions of NMOG or GROC, the needs for this parameter will diminish. However, in cases where VOC and IVOC speciation are provided separately, IVOC/GROC is a powerful metric for stitching together profiles and assessing impacts of profile updates.

In all cases, we assume the methane fraction of the original profile is correct. Therefore, we renormalize all TOG species by (1.0 – CH_4/TOG) to convert to NMOG. For many of the mobile sector sources (e.g. nonroad, evaporative, and others), we begin with this NMOG speciation, remove the IVOCs and SVOCs, and renormalize the remaining species to total GROC by dividing by (1.0 - IVOC/GROC). We add IVOC speciation as discussed in the following paragraph and convert the NMOG speciation back to TOG by normalizing to the original methane fraction (1.0 + CH_4/TOG). Additionally, Lu et al. (2018) provided updated VOC profiles for onroad light duty gasoline, heavy duty diesel, and aircraft turbine engines. These profiles do not include methane, IVOCs, or SVOCs. For sources for which we use these new VOC profiles, we renormalize to total GROC using (1.0 – IVOC/GROC), add IVOC species consistent with the following paragraph, and add methane assuming the methane fraction from the original (i.e. renormalize to 1.0 + CH_4/TOG).

Finally, IVOC speciation of explicit compounds and lumped groups is provided by several studies (Table S3 and Fig. S3) of onroad and nonroad sources. The studies vary in the number of explicit compounds reported, so we have selected 9 compounds that were common among all studies. For most sources, the balance of the IVOC emissions fall in the alkane-like lumped groups according to volatility reported by the study. Lu et al. (2020) parameterized aromatic IVOCs for onroad gasoline sources, which are important SOA precursors. Zhao et al. (2015) reported speciation for onroad and nonroad diesel branched and cyclic compounds, which we have incorporated. One evaporative profile for diesel fuel has been updated as well using data from Gentner et al. (2012) The ROC species have been added to the newest release of SPECIATE. They represent lumped

mixtures of similar hydrocarbons and oxygenates, so they do not have explicit CAS numbers, but SPECIATE IDs have been assigned to them, and they may be used for reporting results of future speciation studies.

The new GROC-compatible VOC profiles appear in Table S4. These profiles include methane and other exempt VOCs. Care must be taken to ensure that these profiles are applied to the proper inventory pollutant.

S5. Particulate Organic Matter sampling and characterization

Current mobile emission models rely on particle emissions data that are typically measured by sampling on filter media and weighing total captured mass offline (Fig. S2) (Fulper et al., 2010; Sonntag et al., 2012). Teflon filters are used for sampling total $PM_{2.5}$ and are often subjected to some level of dilution in a Constant-Volume Sampler to control the temperature and relative humidity of the sample. Inorganic ions and elements are characterized from these filters using solvent extraction and (e.g.) x-ray fluorescence techniques. Elemental and organic carbon are quantified via thermal-optical reflectance of mass collected in parallel on quartz fiber filters. Finally, non-carbon organic matter is either assumed from published ratios of organic matter to organic carbon (Simon et al., 2011) or is assumed to equal the difference between the total $PM_{2.5}$ Teflon filter measurement and the sum of inorganic ions, elements, elemental carbon, and organic carbon (Sonntag et al., 2012). Speciation profiles are integrated into the SPECIATE database and may be referenced using the codes provided in Table S1a. Equation S1 shows how inventory fine PM ($EF_{PM2.5}$; measured on the Teflon filter) is translated to primary organic aerosol emissions (EF_{OM}):

$$EF_{OM} = EF_{PM2.5} * OC_{wt\%} * OM{:}OC_i \quad \text{(S1)}$$

where $OC_{wt\%}$ is the fraction of OC in the SPECIATE profile and $OM{:}OC_i$ is assumed for each source based on reference literature. For mobile sources it is in the range of 1.2-1.3. Emission models and inventories are constrained by total PM measurements across a variety of source attributes and operating conditions because Teflon filter measurements and continuous online PM measurement optical techniques are relatively cheap. Characterizing speciation, on the other hand, is relatively expensive and thus far fewer datasets exists. Frequently, it is challenging to assess the uncertainty introduced when applying a speciation profile to a large fleet of vehicles, for example, or to the same type of vehicle in various operating modes. Where data exist, observed differences can be captured, such as the difference in EC fractional contributions between start and transient modes for heavy duty diesel trucks (46% and 79%, respectively). However, these detailed data are relatively sparse, and more are needed.

Sorptive partitioning artifacts are an additional uncertainty that have been noted for some time (Turpin et al., 1994). It is well-established that SVOCs and IVOCs can adsorb to quartz filters when absorptive partitioning parameterizations would predict them to be mostly or wholly in the gas phase. Research studies recommend using a backup quartz filter behind a Teflon filter to estimate the extent of positive bias from this artifact so that it can be subtracted from the quartz filter OC analysis. Some datasets used in regulatory emission models have accounted for this bias, while others have not, and it is not well-documented. Sonntag et al. (2012) performed this correction on a subset of 10 samples but found that correcting for the artifact led to negative $PM_{2.5}$

emissions because of the low magnitude of particle emissions and potential contamination from silicone tubing.

Dilution artifacts are potentially much more problematic than sorptive artifacts and have been the focus of several research studies across most major mobile source categories (Lu et al., 2018). Because organic compounds are in dynamic equilibrium between the particle and gas phases, their particle-phase emission factors are a function of their total abundance, their vapor pressure, and the dilution rate (i.e. the total organic loading) of the test. The following form of Raoult's Law describes this relationship:

$$C_{i,vap} = \frac{C_{i,ptcl}}{C_{OA}} C_i^* \quad \text{(S2)}$$

where $C_{i,vap}$ and $C_{i,ptcl}$ are the vapor and particle-phase concentrations of species i, C_{OA} is the total concentration of organic particle mass, and C_i^* is the saturation concentration of species i, which is related to the species vapor pressure via the Ideal Gas Law (Donahue et al., 2006). Dozens of studies have measured and parameterized mobile source emissions using this Volatility Basis Set (VBS) framework (e.g. May et al. (2013a, b); Huang et al.(2018); Jathar et al.(2020)). Typically, the approach involves parameterizing the fraction of total organic particle mass across a series of lumped species with increasing saturation concentration. With this information, a partitioning curve can be constructed to assess the degree to which temperature and dilution may impact filter-based test measurements (Robinson et al., 2010). Studies repeatedly find modest variability in the VBS parameters optimized across mobile sources. However, it remains a challenge to understand how to link these new detailed data with existing filter-based particle emission inventory rates. Specifically, it is unclear what C_{OA} is relevant for each OM emission factor presented in Table S1a.

S6. CROC parameterization

We document here the steps taken to translate organic PM emissions output by current mobile models to speciated Condensable Reactive Organic Carbon (CROC), defined as compounds with C^* less than 320 μg m^{-3}. These are SVOCs, LVOCs, ELVOCs, and less volatile compounds. Our approach considers the methods and sources of uncertainty described in section S5 and refines previous approaches that apply VBS parameterizations across all anthropogenic emissions (e.g. Murphy et al. (2009)) or all gasoline and diesel sources (e.g. Koo et al. (2014); Lu et al. (2020)). First, we demonstrate an approach for converting OM emission factors to CROC based on test results from detailed research studies. Second, we document the volatility profiles used to parameterize the resulting CROC emissions.

May et al. (2013b) sampled emissions from a large fleet of 64 onroad gasoline vehicles and quantified simultaneously the organic aerosol concentration (bare quartz and sorptive-artifact-corrected) and the particle-phase emission factor. Lu et al. (2018) combined this data with sorbent tube measurements of total gas plus particle concentration of compounds SVOC and IVOC to yield speciation profiles of total emissions across a comprehensive range of volatility. With the Lu et al. (2018) profiles we can estimate total CROC emissions from the organic aerosol emission factors reported by May et al. (2013b), as shown in equation S3.

$$EF_{CROC} = EF_{OM} \cdot [CROC]/[OM] \quad \text{(S3a)}$$

$$[OM] = \left(\sum_{i=-2}^{5} \frac{f_{10^i}}{1+c^*_{10^i}(T)/C_{OA}} \right) \cdot [ROC_{\leq 10^5}] \quad \text{(S3b)}$$

$$[CROC]/[ROC_{\leq 10^5}] = \frac{f_{CROC}}{f_{\leq 10^5}} \quad \text{(S3c)}$$

$$[CROC]/[OM] = \frac{f_{CROC}}{f_{\leq 10^5}} \left(\sum_{i=-2}^{5} \frac{f_{10^i}}{1+c^*_{10^i}(T)/C_{OA}} \right)^{-1} \quad \text{(S3d)}$$

$$c^*_{10^i}(T) = c^*_{10^i,298\,K} \cdot \left(\frac{298}{T}\right) e^{\frac{-\Delta H_{vap,i}}{R}\left(\frac{1}{T}-\frac{1}{298}\right)} \quad \text{(S3e)}$$

$$\Delta H_{vap,i} = 85 - 11 \cdot log_{10} c^*_{10^i,298\,K} \quad \text{(S3f)}$$

Equation S3a states that we can relate CROC emission factors to OM emission factors using the ratio of calculated total CROC concentration to the OM concentration measured in each test. Equation S3b accounts for partitioning from low volatility species (c* bin centered at 10^{-2} μg m^{-3}) up to IVOCs (c* bin centered at 10^5 μg m^{-3}) and calculates the total gas plus particle mass across this entire volatility range. We select c* = 10^5 μg m^{-3} as a nominal upper bound because higher volatility compounds are not expected to partition significantly to the filter sample and most volatility distributions reported in the literature do not exceed this IVOC bin. It adjusts this total by the ratio $\frac{f_{CROC}}{f_{\leq 10^5}}$ where $f_{\leq 10^5}$ is the total fraction of ROC mass from the c* bin centered at 10^5 μg m^{-3} and below, while f_{CROC} is the fraction of mass from c* bin centered at 100 μg m^{-3} and below, which meets the CROC definition. The c* values used in equation S3d are adjusted for temperature (typically 47 °C) using equation S3e. Enthalpy of vaporization is parameterized in May et al. (2013a,b) as equation S3f. When Eq. S3a-f are applied to systems beyond this study, the upper bound volatility bin in equation S3d may be reduced from c* bin centered at 10^5 μg m^{-3} to a lower volatility bin, as long as it at least includes the c* bin centered at 100 μg m^{-3} so that all CROC is captured.

Figure S4 shows the relationship between organic aerosol emission factor and the estimated CROC emission factors for each test measurement. The CROC emission factors are corrected for temperature dependence using enthalpies of vaporization published by May et al. (2013b). These data are highly correlated in log-log space and are well-described with a power-law function. This function may now be used to estimate total CROC emission factors of onroad gasoline cold start tests. Qualitatively, we see behavior that we would expect in Fig. S5. As the OM filter emission factor decreases, more semivolatile compound mass breaks through the filter. Thus, the correction factor to translate OM emissions to CROC goes up. This is a critical feature of filter-based emission tests. As combustion technologies are made cleaner, there is a perceived accelerating decrease in particle-phase mass because of absorptive partitioning. However, vapor-phase emissions can readily partition back to the particle phase if ambient concentrations are high, temperature are low, or the compounds are oxidized to form SOA. It is crucial to account for this emitted mass. At high OM emission factors, CROC/OM values go below 1.0, indicating IVOCs are contributing significantly to the filter measurement and should be subtracted out, so that only CROC mass is considered. As discussed in section S3, IVOC mass will be considered in the GROC speciation.

We can also derive a relationship for data without artifact corrections (i.e. bare quartz). Figure S6 shows that CROC emission factors can be approximated from uncorrected OM filter emission factors using a piece-wise function segregated at OM emission factor equal to 10 mg kg^{-1} fuel. Below this value, as filter mass decreases, the estimated CROC increases but not as strongly, because adsorbed SVOCs and IVOCs are biasing the OM filter measurement high. At higher OM emission factors, the artifact-corrected and uncorrected data look similar. The coefficients of determination (R^2) in Figs. S6 and S7 reinforce the recommendation that if filters are used to measure OM (or OC) emission factors, artifact-correction using a quartz behind Teflon approach should be prioritized.

We have developed analogous relationships for other key mobile sector sources and operating modes. Lu et al. (2018) reported total volatility profiles for onroad light-duty gasoline hot running conditions, 6 nonroad gasoline engines, 5 heavy duty diesel trucks without particulate filters, 3 heavy duty diesel trucks with particulate filters, and 1 aircraft turbine engine. For these gasoline and diesel sources, we combine the profiles and raw concentration and emission factor data as discussed for onroad gasoline cold starts (Table S6; Figs. S8-S16). Onroad heavy duty diesel with particulate filters are a special case. For bare quartz filter measurements, we use the same approach as for onroad gasoline sources (Fig. S8). For artifact-corrected emission factors, we find that fitting CROC emission factors to OM emission factors with a power law underestimates CROC/OM values at very high OM emission factors. To mitigate this, we instead parameterize the organic aerosol concentration (C_{OA}) as a linear function of OM emission factor and then use VBS partitioning theory to calculate CROC at the sample temperature and OM emission factor (see Table S6).

Nonroad gasoline data were retrieved from Lu et al. (2018) (Fig. S11) and paired with adsorbent tube results for nonroad gasoline. We derive a similar function as that recommended by Lu et al. (2018) (EF_{CROC} = 1.1 * EF_{OM}). However, by using a power law fit, our alternative formulation ($EF_{CROC} = 1.9231 * EF_{OM}^{0.9042}$) reduces unbounded, large enhancements at high OM emission factors, which are characteristic of nonroad gasoline emissions tests (May et al., 2014). Nonroad diesel organic particulate emissions were characterized by Jathar et al. (2020) using both filter measurements as well as tube samples (Figs. S12 and S13). Huang et al. (2018) measured marine emissions using both filter and tubes as well for high sulfur and low sulfur fuels under a variety of cruising and other real-world operating modes (Fig. S14). We have averaged the volatility distributions for the low and high sulfur fuel cases. The organic aerosol concentrations measured in these tests were very high; thus, the relationship of CROC to OM emission factor is essentially linear. More tests need to be conducted at lower concentrations to better constrain cleaner marine engines burning residual oil. For aircraft turbine engines, there are a limited number of OM emission factor measurements (Fig. S15) (Presto et al., 2011). The bare quartz trend is highly nonlinear and will yield unreasonable results at low and high OM emission factor magnitudes. The artifact-corrected trend is more robust but still uncertain, so we opt for a uniform CROC/OM correction of 1.2 (Table S6).

In Table S7, we show the source-specific CROC/OM correction factors resulting from combing the functions derived in Table S6 with the OM emission factors estimated in Table S1a. It is uncertain whether each OM emission factor is artifact-corrected, so we provide both estimates to show the potential impact of that uncertainty. Future work should reexamine these corrections as OM emission factors are updated to reflect newer sources or persisting super emitting sources. For

this first application, we make our best judgement about which sources are artifact corrected. We rely on both the magnitude of the emission factor and features of the speciation profile, like the ratio of EC to OC. We assume that the existing OM emission factors for heavy duty diesel engines with particulate filters are most consistent with artifact-corrected measurements due to their low magnitude and low OM fractional contribution to the total fine PM emission factor (18.7%). We also assume that nonroad diesel sources are artifact-corrected because the CROC/OM function derived from Jathar et al. (2020) would reduce total CROC emissions across this group of sources by approximately a factor of 2. This adjustment might very well be necessary, but more careful consideration of nonroad diesel PM emission factors is needed.

Volatility distributions for C^* ranging from 10^{-2} μg m^{-3} to 10^3 μg m^{-3} are provided in Table S5a to speciate the CROC emission factors to alkane-like lumped species. Figure S16 (top) shows that most of the distributions describe relatively similar behavior, although differences are important to capture. The obvious outlier is marine residual oil emissions; Huang et al. (2018) found that about half of the CROC emissions were in the $C^* = 10^{-2}$ μg m^{-3} bin. Table S5b and Fig. S16 (bottom) depict the volatility distributions of the same sources but expanded to the IVOC range ($C^* < 3.2 \times 10^5$ μg m^{-3}). It is interesting to compare the parameters prescribed for onroad diesel in May et al. (2013a) to those published for onroad diesel in Lu et al. (2018) Notably, the fraction of mass attributed to IVOCs in the former is much smaller than that from the latter. This apparent inconsistency is a result of May et al. (2013a) parameters defined to explain mass captured on the filter, and thus neglecting most of the IVOC mass. Lu et al. (2018) parameters, meanwhile, consider both particle and gas-phase mass for the entire volatility spectrum. Figure S16 demonstrates that the range of volatility bins considered impacts the shape of the partitioning curve. Future studies reporting VBS parameters and partitioning curves need to be clear about the context of the underlying data or risk misapplication in inventories and models.

The new CROC-compatible PM speciation profiles appear in Table S8. These profiles sum to 100%, but in practice, the reactive organic carbon species (species #3394-3398) are multiplied by the CROC/OM ratio from Table S7 when applied in the emission inventory speciation step. Thus, depending on the contribution of organic species to the PM profile and the value of the CROC/OM ratio, the new profile total may be above or below 100%. This deviation is intended to address biases in partitioning and filter artifacts.

S7. Adjustment to SOA from VCPs

The VCP emissions provided by the VCPy tool (Seltzer et al., 2021) include speciated and lumped VOCs and lumped IVOCs. Pennington et al. (2021) analyzed SOA formation from nonoxygenated alkane IVOCs, aromatic IVOCs, oxygenated IVOCs, and siloxanes. CMAQ simulations predicted that nonoxygenated (alkane plus aromatic) IVOCs contributed the most to total SOA in southern California, with a 29% effective SOA yield, followed by VOC species. Oxygenated IVOCs contributed a small portion, with a 6.28% effective SOA yield. Siloxanes contributed minimally to total SOA. The CMAQ-ROC simulations did not distinguish between oxygenated and nonoxygenated IVOC emissions, so we reduced the predicted VCP SOA to account for the impact of representing the oxygenated IVOCs with a 29% effective SOA yield. Equations S4 and S5 describe the correction we applied.

$$X_{IVOC}^{SOA} = \frac{y_{Oxy} f_{Oxy} + y_{NonOxy} f_{NonOxy}}{y_{NonOxy}} = \frac{0.0628 * 0.52 + 0.29 * 0.48}{0.29} = 0.586 \quad \text{(S4)}$$

$$X_{VCP}^{SOA} = \frac{X_{IVOC}^{SOA} \cdot P_{IVOC}^{SOA} + P_{VOC}^{SOA}}{P_{IVOC}^{SOA} + P_{VOC}^{SOA}} = \frac{0.586 * 490 + 110}{490 + 110} = 66.2\% \quad \text{(S5)}$$

where X_{IVOC}^{SOA} is the correction applied to SOA produced by VCP IVOCs, X_{VCP}^{SOA} is the correction applied to total SOA from VCPs, y_{Oxy} is the oxygenated IVOC effective SOA yield, y_{NonOxy} is the nonoxygenated IVOC effective yield, f_{Oxy} is the fraction of VCP IVOC emissions that are oxygenated, f_{NonOxy} is the fraction of nonoxygenated IVOCs from VCPs, CMAQ-predicted (domain-wide annual average) P_{IVOC}^{SOA} is the production rate of SOA from IVOCs assuming all VCP IVOCs are nonoxygenated, and P_{VOC}^{SOA} is the CMAQ-predicted production rate of SOA from VCP VOCs. Using this representative calculation, we subtracted 33.8% of the mass concentration from VCP SOA.

S8. Evaluation within the South Coast Air Basin

Because of the importance of mobile source emissions for O_3 and PM exceedances, more detailed historical measurements for ROC components exist at sites within the South Coast Air Basin (SOCAB) in southern California. Zhao et al. (2022) compiled measurement and modeling data for 2008-2019 for total organic aerosol and estimated the contribution of POA and SOA using an OC/EC source apportionment approach. In 2017, that study estimated an average SOA concentration of 3.6 μg m^{-3} and a POA concentration of 1.43 μg m^{-3} at the Los Angeles Air Quality System (AQS) site, yielding an SOA fraction of 72%. The CMAQ mobile ROC simulation predicts annual SOA and POA concentrations equal to 2.23 and 2.26 μg m^{-3}, resulting in an SOA fraction of 49.6%. This comparison is based on hourly CMAQ data for the entire year 2017, not paired in time with the AQS observations. Figure S36 confirms that when organic carbon (OC) predictions are paired in time with the AQS data, they reproduce measurements well.

Ambient IVOC measurements in the South Coast Air Basin do not exist in 2017 to our knowledge. CMAQ predicts annual and summertime ambient IVOC concentrations of 11.3 and 10.9 μg m^{-3} at Pasadena. A CMAQ simulation with mobile source emissions set to zero suggests that 0.98 and 1.21 μg m^{-3} of IVOCs are attributable to mobile sources annually and during the summer, respectively. Zhao et al. (2022) report that mobile source NMOG declines by about 38% from 2010 to 2017. Volatile chemical product (VCP) NMOG emissions are expected to have been much more stable during that time period (4% decrease). Assuming, for the purposes of comparison, that mobile and non-mobile IVOC concentrations scale linearly with NMOG emissions backward in time, the approximate total IVOC concentrations in summer 2010 would be 11.3 μg m^{-3}. This is similar to the IVOC measured (10.5 μg m^{-3}) at Pasadena during May and June 2010 (Zhao et al., 2014).

The sum of mobile IVOC emissions throughout the SOCAB domain is 12 tons day^{-1}, while it is 84 tons day^{-1} for VCP sources. Extrapolating these values back to 2010 yields a mobile IVOC emission total of 19.7 tons day^{-1} and VCP emission equal to 87.5 tons day^{-1}. The CMAQ-ROC mobile IVOC emission rate is 71% of that estimated previously by Lu et al. (2020) using CMAQ for the CalNex period (27.6 tons day^{-1}). That study reported that a nonmobile IVOC emission rate of 68.5 tons day^{-1}. The total IVOC emissions rate in SOCAB from Lu et al. (2020) (96.1 tons day^{-1}) led to an average IVOC concentration of ~14 μg m^{-3} at Pasadena.

S9. Production

Organic aerosol production occurs via direct primary particle emissions and secondary aerosol formation. The updated mobile ROC emissions and CMAQ photochemical results allow us to separately estimate the POA emission (after partitioning) and SOA production normalized to nonvolatile OM and NMOG emissions respectively. Table S11a quantifies the corrected emission of ambient POA as a function of conventional OM emissions averaged across the model domain. This quantity varies seasonally from 0.515 to 0.710 g POA $(g\,OM)^{-1}$. SOA production varies more strongly, from a low of 0.09 g SOA $(g\,NMOG)^{-1}$ in winter to 0.132 g SOA $(g\,NMOG)^{-1}$ in summer. The total OA production varies from 0.114 to 0.146 throughout the year.

Likewise, CMAQ model results can quantify the average concentration of POA and SOA expected as a function conventional OM and NMOG emissions, respectively. This relationship for POA is relatively flat throughout the year, varying from 30.2 to 34.8 $\mu g\ m^{-3}$ POA $(kg\ hr^{-1}\ OM)^{-1}$. SOA concentrations vary from 4.8 to 8.2 $\mu g\ m^{-3}$ POA $(kg\ hr^{-1}\ NMOG)^{-1}$. These simplified production rates and concentration response factors are not intended for rigorous photochemical modeling applications but may be used for estimating the impact of specific sources in simplified frameworks like the EPA COBRA model (https://www.epa.gov/cobra).

S10. Support for legacy emission input datasets

Future air quality modeling studies should rely on mobile emission inputs with the bottom-up considerations we have discussed in this work. However, in some cases, practical needs require that existing emissions datasets be projected to be compatible with contemporary chemical mechanisms. For example, model studies in the near future may need to scale total NMOG for mobile sources to populate emissions for alkane and aromatic IVOCs. To support these needs, we provide scale factors in Table S12 that prescribe the mapping of the key model species added to the Carbon Bond chemical mechanism for several levels of aggregation in including all mobile sources, mobile sources excluding marine vessels, onroad sources, nonroad sources, etc. For each example, the mean scale factor and standard deviation across the spatial domain are provided to illustrate the relative uncertainty in each parameter.

Although we provide these data, we urge caution when applying them to large domains and across multiple years. These factors are applicable to the 2017 calendar year and extrapolation more than 10 years into the past is not recommended. New scale factors should be calculated for historical applications. As shown in Fig. S40, the variability in IVOC/NMOG and CROC/OM is substantial when all mobile sources are considered together, and this relaxes considerably when marine vessels are excluded. If existing emission inputs are available for gasoline and diesel sources separately, less uncertainty is introduced from using suggested scale factors, especially if marine sources can be treated separately from the rest of the diesel-fueled fleet.

References

Ayala, A., Gebel, M. E., Okamoto, R. A., Rieger, P. L., Kado, N. Y., Cotter, C., and Verma, N.: Oxidation catalyst effect on cng transit bus emissions, SAE Technical Paper0148-7191, 10.4271/2003-01-1900, 2003.

Corbin, J. C., Pieber, S. M., Czech, H., Zanatta, M., Jakobi, G., Massabo, D., Orasche, J., El Haddad, I., Mensah, A. A., Stengel, B., Drinovec, L., Mocnik, G., Zimmermann, R., Prevot, A. S. H., and Gysel, M.: Brown and black carbon emitted by a marine engine operated on heavy fuel oil and distillate fuels: Optical properties, size distributions, and emission factors, J Geophys Res-Atmos, 123, 6175-6195, 10.1029/2017jd027818, 2018.

Donahue, N. M., Robinson, A. L., Stanier, C. O., and Pandis, S. N.: Coupled partitioning, dilution, and chemical aging of semivolatile organics, Environ Sci Technol, 40, 2635-2643, 10.1021/es052297c, 2006.

Fulper, C. R., Kishan, S., Baldauf, R. W., Sabisch, M., Warila, J., Fujita, E. M., Scarbro, C., Crews, W. S., Snow, R., and Gabele, P.: Methods of characterizing the distribution of exhaust emissions from light-duty, gasoline-powered motor vehicles in the us fleet, Journal of the Air & Waste Management Association, 60, 1376-1387, 10.3155/1047-3289.60.11.1376, 2010.

Gentner, D. R., Isaacman, G., Worton, D. R., Chan, A. W., Dallmann, T. R., Davis, L., Liu, S., Day, D. A., Russell, L. M., Wilson, K. R., Weber, R., Guha, A., Harley, R. A., and Goldstein, A. H.: Elucidating secondary organic aerosol from diesel and gasoline vehicles through detailed characterization of organic carbon emissions, Proc Natl Acad Sci U S A, 109, 18318-18323, 10.1073/pnas.1212272109, 2012.

Gierczak, C. A., Kralik, L. L., Mauti, A., Harwell, A. L., and Maricq, M. M.: Measuring nmhc and nmog emissions from motor vehicles via ftir spectroscopy, Atmospheric Environment, 150, 425-433, 10.1016/j.atmosenv.2016.11.038, 2017.

Gordon, T. D., Tkacik, D. S., Presto, A. A., Zhang, M., Jathar, S. H., Nguyen, N. T., Massetti, J., Truong, T., Cicero-Fernandez, P., Maddox, C., Rieger, P., Chattopadhyay, S., Maldonado, H., Maricq, M. M., and Robinson, A. L.: Primary gas- and particle-phase emissions and secondary organic aerosol production from gasoline and diesel off-road engines, Environ Sci Technol, 47, 14137-14146, 10.1021/es403556e, 2013.

Harrell, M. and Janssen, M.: 2014 ertac rail locomotive emission inventories for the united states [dataset], 2017.

Huang, C., Hu, Q., Li, Y., Tian, J., Ma, Y., Zhao, Y., Feng, J., An, J., Qiao, L., Wang, H., Jing, S., Huang, D., Lou, S., Zhou, M., Zhu, S., Tao, S., and Li, L.: Intermediate volatility organic compound emissions from a large cargo vessel operated under real-world conditions, Environ Sci Technol, 52, 12934-12942, 10.1021/acs.est.8b04418, 2018.

Jathar, S. H., Friedman, B., Galang, A. A., Link, M. F., Brophy, P., Volckens, J., Eluri, S., and Farmer, D. K.: Linking load, fuel, and emission controls to photochemical production of secondary organic aerosol from a diesel engine, Environ Sci Technol, 51, 1377-1386, 10.1021/acs.est.6b04602, 2017.

Jathar, S. H., Sharma, N., Galang, A., Vanderheyden, C., Takhar, M., Chan, A. W. H., Pierce, J. R., and Volckens, J.: Measuring and modeling the primary organic aerosol volatility from a modern non-road diesel engine, Atmospheric Environment, 223, 117221, 10.1016/j.atmosenv.2019.117221, 2020.

Koo, B., Knipping, E., and Yarwood, G.: 1.5-dimensional volatility basis set approach for modeling organic aerosol in camx and cmaq, Atmospheric Environment, 95, 158-164, 10.1016/j.atmosenv.2014.06.031, 2014.

Lu, Q., Murphy, B. N., Qin, M., Adams, P. J., Zhao, Y., Pye, H. O. T., Efstathiou, C., Allen, C., and Robinson, A. L.: Simulation of organic aerosol formation during the calnex study: Updated mobile emissions and secondary organic aerosol parameterization for

intermediate-volatility organic compounds, Atmos Chem Phys, 20, 4313-4332, 10.5194/acp-20-4313-2020, 2020.
Lu, Q. Y., Zhao, Y. L., and Robinson, A. L.: Comprehensive organic emission profiles for gasoline, diesel, and gas-turbine engines including intermediate and semi-volatile organic compound emissions, Atmospheric Chemistry and Physics, 18, 17637-17654, 10.5194/acp-18-17637-2018, 2018.
May, A. A., Presto, A. A., Hennigan, C. J., Nguyen, N. T., Gordon, T. D., and Robinson, A. L.: Gas-particle partitioning of primary organic aerosol emissions: (2) diesel vehicles, Environ Sci Technol, 47, 8288-8296, 10.1021/es400782j, 2013a.
May, A. A., Presto, A. A., Hennigan, C. J., Nguyen, N. T., Gordon, T. D., and Robinson, A. L.: Gas-particle partitioning of primary organic aerosol emissions: (1) gasoline vehicle exhaust, Atmospheric Environment, 77, 128-139, 10.1016/j.atmosenv.2013.04.060, 2013b.
May, A. A., Nguyen, N. T., Presto, A. A., Gordon, T. D., Lipsky, E. M., Karve, M., Gutierrez, A., Robertson, W. H., Zhang, M., Brandow, C., Chang, O., Chen, S. Y., Cicero-Fernandez, P., Dinkins, L., Fuentes, M., Huang, S. M., Ling, R., Long, J., Maddox, C., Massetti, J., McCauley, E., Miguel, A., Na, K., Ong, R., Pang, Y. B., Rieger, P., Sax, T., Truong, T., Vo, T., Chattopadhyay, S., Maldonado, H., Maricq, M. M., and Robinson, A. L.: Gas- and particle-phase primary emissions from in-use, on-road gasoline and diesel vehicles, Atmospheric Environment, 88, 247-260, 10.1016/j.atmosenv.2014.01.046, 2014.
McDonald, J., Osborne, D., and Khalek, I.: The composition of particulate matter emissions from two tier 2 locomotives, Proceedings of the Air and Waste Management Association's annual conference and exhibition,
Murphy, B. N. and Pandis, S. N.: Simulating the formation of semivolatile primary and secondary organic aerosol in a regional chemical transport model, Environ Sci Technol, 43, 4722-4728, 10.1021/es803168a, 2009.
National Emissions Inventory Collaborative: 2016v1 emissions modeling platform [dataset], 2019.
Pennington, E. A., Seltzer, K. M., Murphy, B. N., Qin, M., Seinfeld, J. H., and Pye, H. O.: Modeling secondary organic aerosol formation from volatile chemical products, Atmospheric chemistry and physics, 21, 18247-18261, 10.5194/acp-21-18247-2021, 2021.
Presto, A. A., Nguyen, N. T., Ranjan, M., Reeder, A. J., Lipsky, E. M., Hennigan, C. J., Miracolo, M. A., Riemer, D. D., and Robinson, A. L.: Fine particle and organic vapor emissions from staged tests of an in-use aircraft engine, Atmospheric Environment, 45, 3603-3612, 10.1016/j.atmosenv.2011.03.061, 2011.
Robinson, A. L., Grieshop, A. P., Donahue, N. M., and Hunt, S. W.: Updating the conceptual model for fine particle mass emissions from combustion systems allen l. Robinson, Journal of the Air & Waste Management Association, 60, 1204-1222, 10.3155/1047-3289.60.10.1204, 2010.
Seltzer, K. M., Pennington, E., Rao, V., Murphy, B. N., Strum, M., Isaacs, K. K., and Pye, H. O. T.: Reactive organic carbon emissions from volatile chemical products, Atmos Chem Phys, 21, 5079-5100, 10.5194/acp-21-5079-2021, 2021.

Simon, H., Bhave, P. V., Swall, J. L., Frank, N. H., and Malm, W. C.: Determining the spatial and seasonal variability in om/oc ratios across the us using multiple regression, Atmospheric Chemistry and Physics, 11, 2933-2949, 10.5194/acp-11-2933-2011, 2011.
Sonntag, D. B., Bailey, C. R., Fulper, C. R., and Baldauf, R. W.: Contribution of lubricating oil to particulate matter emissions from light-duty gasoline vehicles in kansas city, Environ Sci Technol, 46, 4191-4199, 10.1021/es203747f, 2012.
Turpin, B. J., Huntzicker, J. J., and Hering, S. V.: Investigation of organic aerosol sampling artifacts in the los-angeles basin, Atmospheric Environment, 28, 3061-3071, 10.1016/1352-2310(94)00133-6, 1994.
U.S. EPA: Emission factors for locomotives, 2009.
U.S. EPA: Speciation profiles and toxic emission factors for nonroad engines in moves2014b, 2018.
U.S. EPA: Air toxic emissions from onroad vehicles in moves3, 2020a.
U.S. EPA: Speciation of total organic gas and particulate matter emissions from onroad vehicles in moves3, 2020b.
U.S. EPA: Exhaust emission rates for light-duty onroad vehicles in moves3, 2020c.
U.S. EPA: Exhaust emission rates of heavy-duty onroad vehicles in moves3, 2020d.
U.S. EPA: 2017 national emissions inventory (nei): January 2021 updated release, technical support document, 2021a.
U.S. EPA: Overview of epa's motor vehicle emission simulator (moves3), 2021b.
U.S. EPA: Engine testing procedures. Cfr, part 1065, title 40, 2022.
Zhao, Y., Tkacik, D. S., May, A. A., Donahue, N. M., and Robinson, A. L.: Mobile sources are still an important source of secondary organic aerosol and fine particulate matter in the los angeles region, Environmental Science & Technology, 56, 15328-15336, 10.1021/acs.est.2c03317, 2022.
Zhao, Y., Nguyen, N. T., Presto, A. A., Hennigan, C. J., May, A. A., and Robinson, A. L.: Intermediate volatility organic compound emissions from on-road diesel vehicles: Chemical composition, emission factors, and estimated secondary organic aerosol production, Environ Sci Technol, 49, 11516-11526, 10.1021/acs.est.5b02841, 2015.
Zhao, Y., Nguyen, N. T., Presto, A. A., Hennigan, C. J., May, A. A., and Robinson, A. L.: Intermediate volatility organic compound emissions from on-road gasoline vehicles and small off-road gasoline engines, Environ Sci Technol, 50, 4554-4563, 10.1021/acs.est.5b06247, 2016.
Zhao, Y., Hennigan, C. J., May, A. A., Tkacik, D. S., de Gouw, J. A., Gilman, J. B., Kuster, W. C., Borbon, A., and Robinson, A. L.: Intermediate-volatility organic compounds: A large source of secondary organic aerosol, Environ Sci Technol, 48, 13743-13750, 10.1021/es5035188, 2014.

Table S6. Functions for determining CROC emission factors given OM emission factors in mg kg^{-1} fuel, assuming particle emissions were characterized on quartz fiber filters.

Source	Filter Method	EF_{CROC} Formulation	References
Gasoline_Cold_Start	Artifact-Corrected	$4.438 * EF_{OM}^{0.7598}$	May et al.(2013a) Lu et al. (2018)
	Bare Quartz	$0.267 * EF_{OM}^{1.8044}$: $EF_{OM} < 10\ mg\ kg^{-1}$ $1.888 * EF_{OM}^{0.9139}$: $EF_{OM} \geq 10\ mg\ kg^{-1}$	
Gasoline_Hot_Running	Artifact-Corrected	$3.332 * EF_{OM}^{0.7947}$	May et al.(2013a) Lu et al. (2018)
	Bare Quartz	$0.189 * EF_{OM}^{1.8504}$: $EF_{OM} < 10\ mg\ kg^{-1}$ $1.273 * EF_{OM}^{0.9745}$: $EF_{OM} \geq 10\ mg\ kg^{-1}$	
Diesel_NonDPF	Artifact-Corrected	$1.036 * EF_{OM}^{1.0453}$	May et al.(2013b) Lu et al. (2018)
	Bare Quartz	$1.033 * EF_{OM}^{0.9706}$	
Diesel_DPF	Artifact-Corrected	Eq. S3 with $C_{OA} = 7.37 * EF_{OM}$	May et al.(2013b) Lu et al. (2018)
	Bare Quartz	$8.005 * EF_{OM}^{0.3593}$	
Gasoline_Nonroad	Bare Quartz	$1.923 * EF_{OM}^{0.9042}$	Lu et al. (2018)
Diesel_Nonroad_NonDPF	Artifact-Corrected	$2.456 * EF_{OM}^{0.8506}$	Jathar et al. (2020)
	Bare Quartz	$0.153 * EF_{OM}^{1.1849}$	
Diesel_Nonroad_DPF	Artifact-Corrected	$1.544 * EF_{OM}^{0.9305}$	Jathar et al. (2020)
	Bare Quartz	$0.466 * EF_{OM}$	
ResidualOil_Marine	Bare Quartz	$0.749 * EF_{OM}$	Huang et al. (2018)
Gas_Turbine_Aircraft	Artifact-Corrected	$1.2 * EF_{OM}$	Presto et al. (2011)

Table S7. Source-dependent CROC/OM factors calculated for this study based on published partitioning curves for bare quartz and sorptive artifact corrected data. Selected CROC/OM parameters are bolded.

Source	Source_Name	CROC/OM Function	EF_OM (mg/kg)	Artifact Corrected CROC/OM	Bare Quartz CROC/OM	Filter Method
1	Pre-Tier 2 E10 Exhaust; Gasoline pre2004; Cold Start	Gas_Cold_Start	149.2	**1.33**	1.23	Artifact Corrected
2	Tier 2 E10 Exhaust; Gasoline 2001-2004; Cold Start	Gas_Cold_Start	54.1	**1.70**	1.34	Artifact Corrected
3	Tier 2 E10 Exhaust; Gasoline 2004+; Cold Start	Gas_Cold_Start	17.9	**2.22**	1.47	Artifact Corrected
4	Pre-Tier 2 E10 Exhaust; Gasoline pre2004; Hot Stabilized Running	Gas_Hot_Running	74.4	**1.37**	1.14	Artifact Corrected
5	Tier 2 E10 Exhaust; Gasoline 2001-2004; Hot Stabilized Running	Gas_Hot_Running	24.6	**1.72**	1.17	Artifact Corrected
6	Tier 2 E10 Exhaust; Gasoline 2004+; Hot Stabilized Running	Gas_Hot_Running	5.6	**2.33**	0.82	Artifact Corrected
7	Conventional Heavy Duty Diesel Exhaust - Idle, pre-2007; Non-DPF	Diesel_NonDPF	1398.4	**1.44**	0.84	Artifact Corrected
8	Conventional Heavy Duty Diesel Exhaust - pre-2007; pre-DPF; start	Diesel_NonDPF	387.9	**1.36**	0.87	Artifact Corrected
9	Conventional Heavy Duty Diesel Exhaust - pre-2007; pre-DPF; running	Diesel_NonDPF	391.1	**1.36**	0.87	Artifact Corrected
10	Heavy Duty Diesel Exhaust, 2007-2009; DPF	Diesel_DPF	11.4	2.21	**1.68**	Bare Quartz
11	Heavy Duty Diesel Exhaust, 2010+; DPF+SCR	Diesel_DPF	3.0	4.53	**3.96**	Bare Quartz
12	CNG - no aftertreatment	Gas_Hot_Running	17.0	1.85	**1.18**	Bare Quartz
13	CNG – oxidation catalyst	Gas_Hot_Running	4.4	2.45	**0.67**	Bare Quartz
14	Tier 2 E85 Exhaust; Cold Start	Gas_Cold_Start	7.2	2.76	**1.30**	Bare Quartz
15	Tier 2 E85 Exhaust; Hot Running	Gas_Hot_Running	3.6	2.56	**0.55**	Bare Quartz
16	SI 2-stroke E0	Gas_Nonroad	6093.9	0.83	**0.83**	Bare Quartz
17	SI 2-stroke E10	Gas_Nonroad	6093.9	0.83	**0.83**	Bare Quartz
18	SI 4-stroke E0	Gas_Nonroad	233.0	1.14	**1.14**	Bare Quartz
19	SI 4-stroke E10	Gas_Nonroad	233.0	1.14	**1.14**	Bare Quartz
20	CI Tier 0	Diesel_Nonroad_NonDPF	2348.2	**0.77**	0.64	Artifact Corrected
21	CI Tier 1	Diesel_Nonroad_NonDPF	1065.9	**0.87**	0.56	Artifact Corrected

Source	Source_Name	CROC/OM Function	EF_OM (mg/kg)	Artifact Corrected CROC/OM	Bare Quartz CROC/OM	Filter Method
22	CI Tier 2	Diesel_Nonroad_NonDPF	538.7	**0.96**	0.49	Artifact Corrected
23	CI Tier 3	Diesel_Nonroad_NonDPF	643.2	**0.94**	0.51	Artifact Corrected
24	CI Tier 4; No DPF	Diesel_Nonroad_NonDPF	149.8	**1.16**	0.39	Artifact Corrected
25	CI Tier 4 DPF; no SCR	Diesel_Nonroad_DPF	3.8	1.41	**0.47**	Bare Quartz
26	CI Tier 4 DPF + SCR	Diesel_Nonroad_DPF	2.6	1.45	**0.47**	Bare Quartz
27	CNG - Oxidation Catalyst	Gas_Hot_Running	141.9	1.20	**1.12**	Bare Quartz
28	LPG Exhaust	Gas_Hot_Running	137.1	1.21	**1.12**	Bare Quartz
29	Airports: AGS gas	Gas_Hot_Running	154.0	1.18	**1.12**	Bare Quartz
30	Airports: AGS diesel	Diesel_NonDPF	121.9	**1.29**	0.90	Artifact Corrected
31	Airports: Aircraft Aviation Gasoline	Gas_Turbine	15.0	**1.20**	1.20	Artifact Corrected
32	Airports: Aircraft Jetfuel	Gas_Turbine	15.0	**1.20**	1.20	Artifact Corrected
33	Class I Line Haul	Diesel_NonDPF	730.6	**1.40**	0.85	Artifact Corrected
34	Class II/III Line Haul	Diesel_NonDPF	793.2	**1.40**	0.85	Artifact Corrected
35	Commuter	Diesel_NonDPF	389.6	**1.36**	0.87	Artifact Corrected
36	Passenger	Diesel_NonDPF	389.6	**1.36**	0.87	Artifact Corrected
37	Yard Locomotives	Diesel_NonDPF	797.2	**1.40**	0.85	Artifact Corrected
38	CMV diesel	Diesel_NonDPF	375.1	**1.36**	0.87	Artifact Corrected
39	CMV residual	Diesel_NonDPF	2695.0	1.48	**0.82**	Bare Quartz

Table S9. Annual total gas and particle mobile emissions (in kt yr^{-1}) for 2017 inventory in the EQUATES and updated (ROC) cases.

	NMOG		EC		OA	
Sub-Sector	**EQUATES**	**CMAQ_ROC**	**EQUATES**	**CMAQ_ROC**	**EQUATES (OM)[1]**	**CMAQ_ROC (CROC)[2]**
Onroad Gas	1,144	1,144	6.71	5.34	15.96	23.02
Onroad Diesel	139	139	37.85	37.49	18.55	25.65
Nonroad Gas	1,001	1,001	4.91	4.57	21.61	20.16
Nonroad Diesel	74	74	45.07	27.20	12.86	21.78
Air	54	54	2.93	0.62	2.02	4.34
Marine	49	49	11.26	7.52	16.74	18.39
Rail	26	26	11.97	7.20	3.41	9.02
Total	2,485	2,485	120.70	89.94	91.13	122.37
%Change		0%		-25%		+34%

[1]The conventional POA emissions are the sum of particulate organic carbon and non-carbon organic matter.
[2]CROC emissions are total particulate and vapor emissions corresponding to the sum of ELVOC, LVOC, and SVOC compounds as defined in the main text.

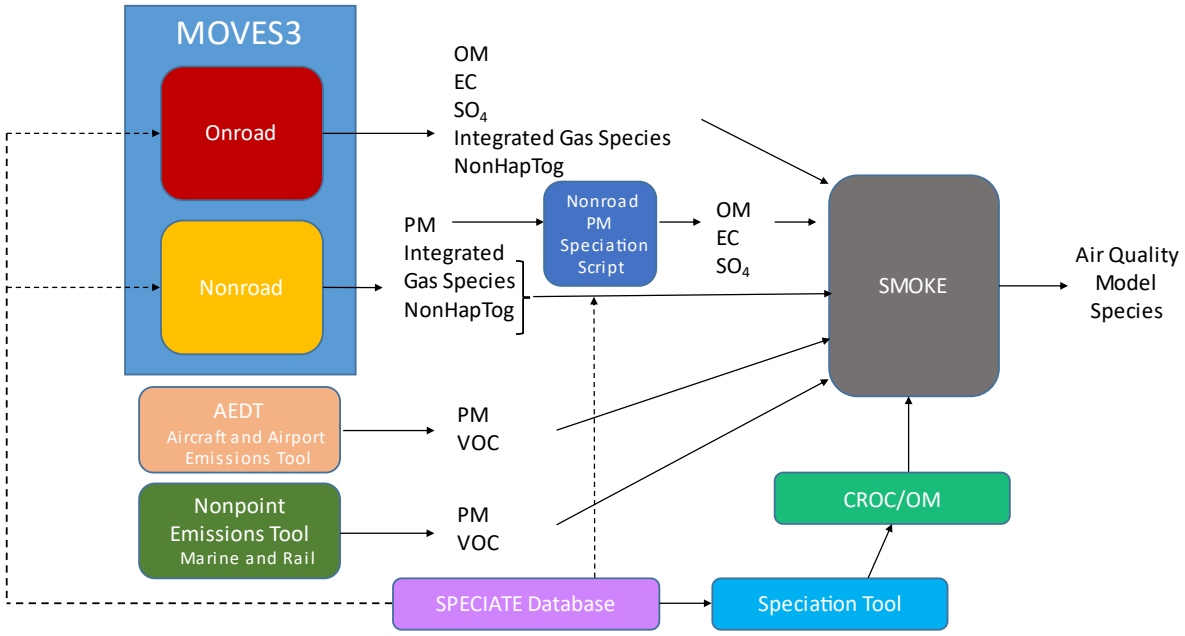

Figure S1. Conceptual diagram of mobile emission models with key inputs and outputs.

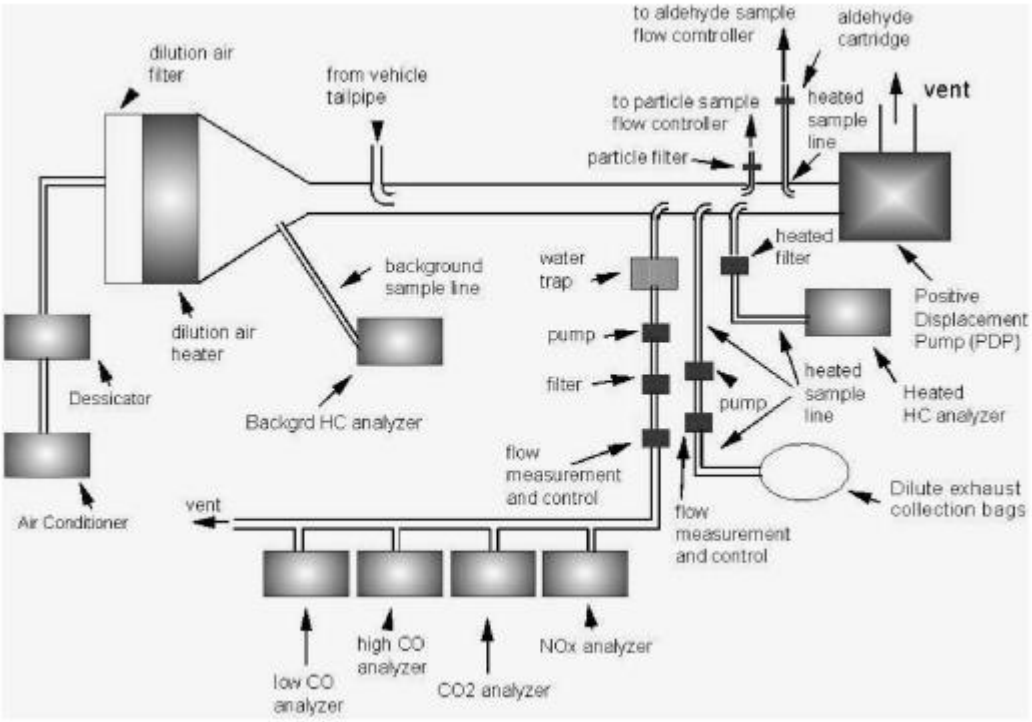

Figure S2. Example schematic of typical configuration for mobile emissions sampling (Fulper et al., 2010).

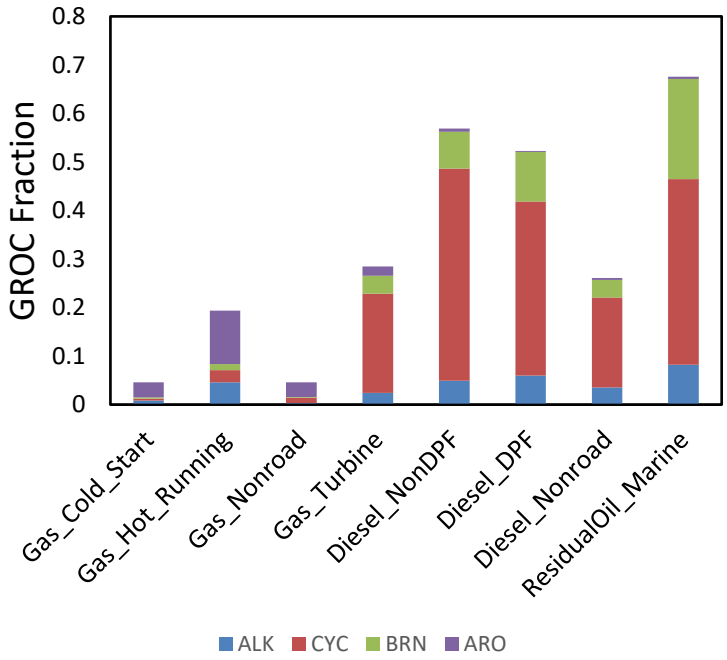

Figure S3. Fractional contribution to total GROC of IVOC chemical classes for the profile types appearing in Tables S2 and S3. The data in this plot is reproduced in greater detail in Table S3 multiplied by the IVOC/GROC fractions in Table S2. Chemical classes include linear alkanes (ALK), non-aromatic cyclic alkanes (CYC), branched alkanes (BRN), and aromatics (ARO).

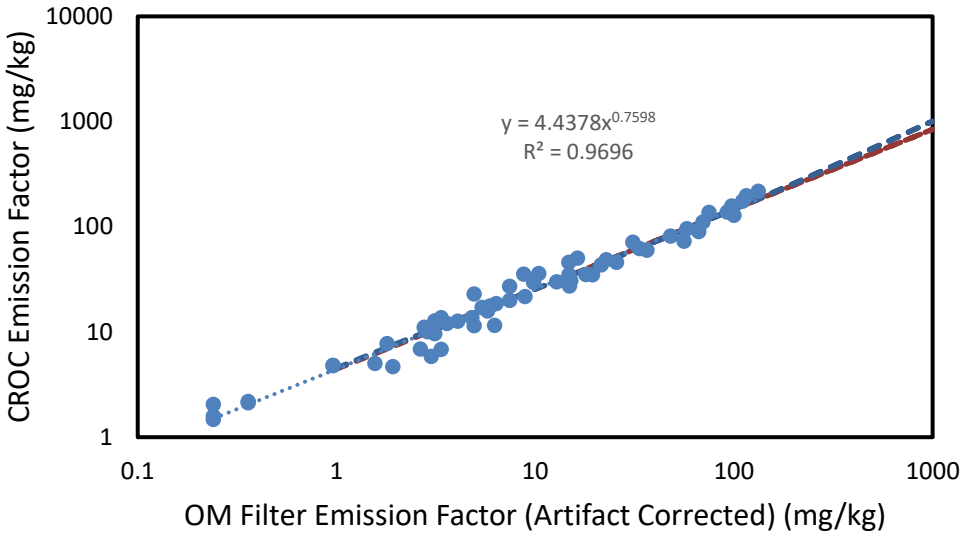

Figure S4. Relationship between artifact-corrected organic particle emission factor (OC*1.2) and CROC emission factor in mg kg^{-1} fuel for onroad light-duty gasoline vehicles during cold-start.

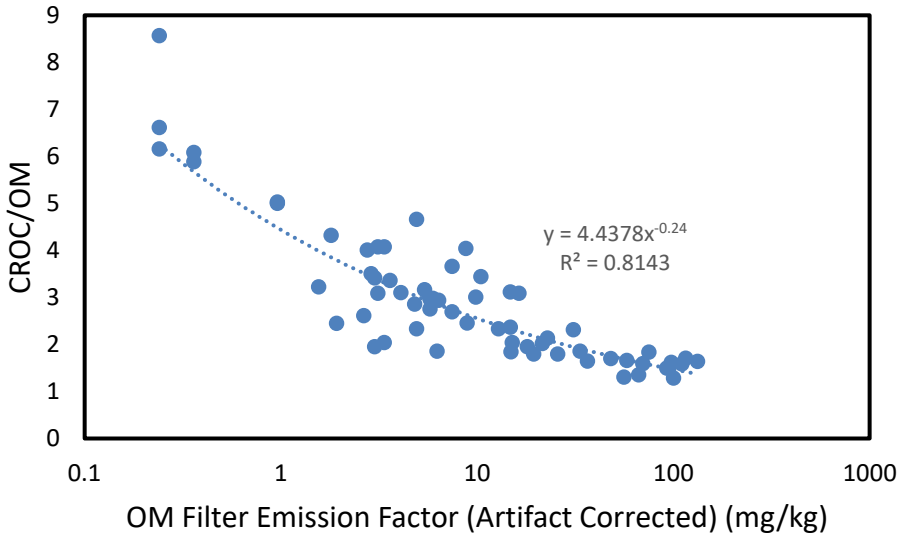

Figure S5. Ratio of CROC emission factor to OM emission factor as a function of OM emission factor (artifact-corrected) for onroad light-duty gasoline vehicles during cold starts.

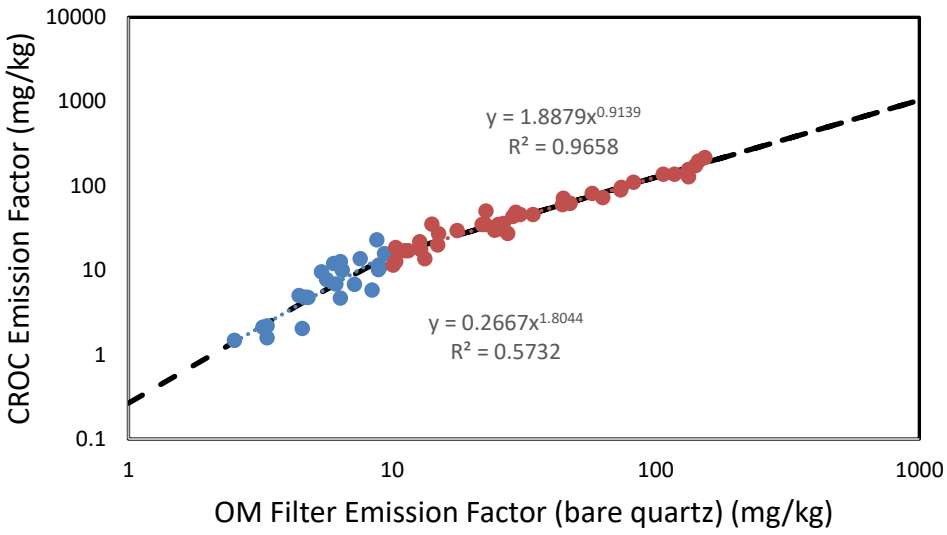

Figure S6. Relationship between bare quartz organic particle emission factor (OC*1.2) and CROC emission factor in mg kg^{-1} fuel for onroad light-duty gasoline vehicles during cold-start.

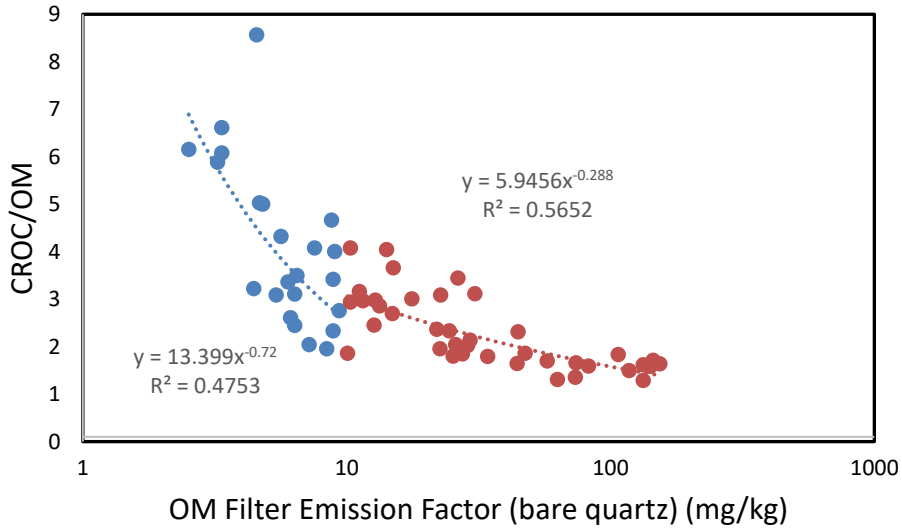

Figure S7. Ratio of CROC emission factor to filter-based particle OM emission factor (OC*1.2) as a function of the latter for onroad light-duty gasoline vehicles during cold starts.

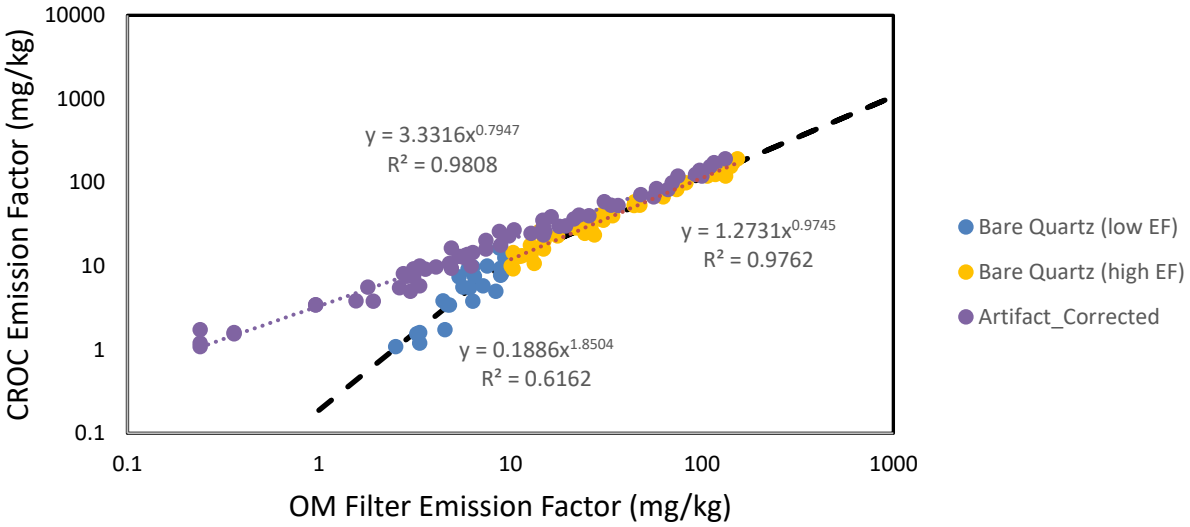

Figure S8. CROC Emission Factor as a function of OM filter emission factors for bare quartz and artifact-corrected data from onroad light duty gasoline hot running conditions.

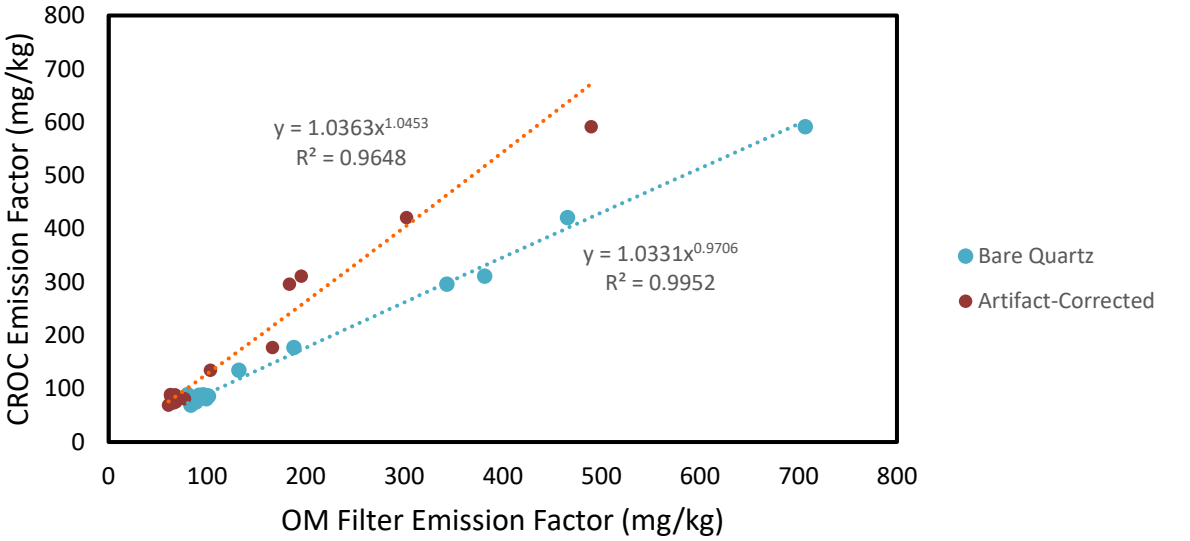

Figure S9. CROC emissions factors as a function of filter-based OM emission factors for onroad heavy duty diesel engines without particulate filters (non-DPF).

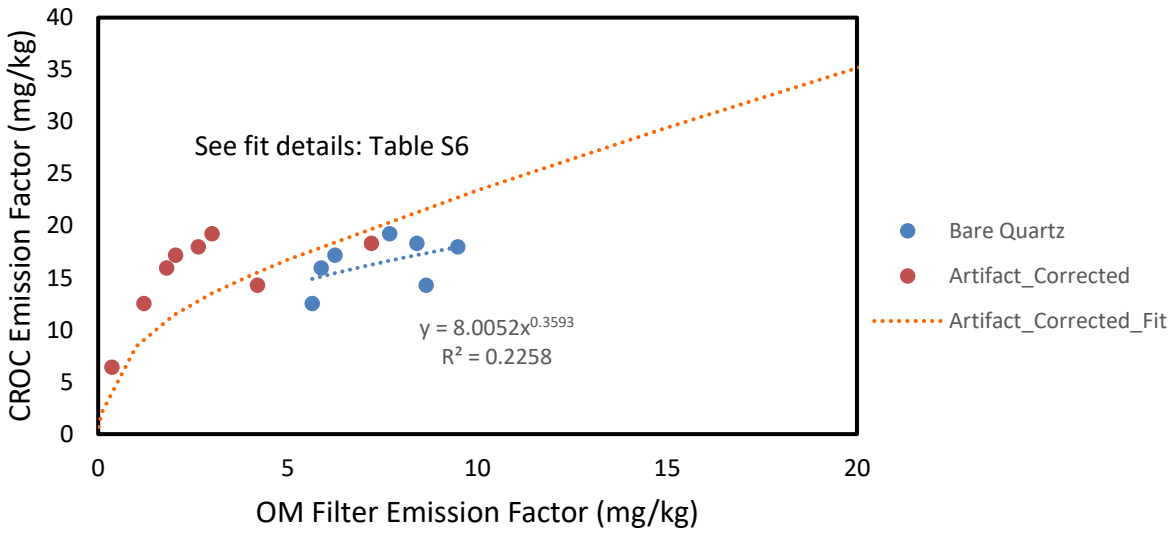

Figure S10. CROC emissions factors as a function of filter-based OM emission factors for onroad heavy duty diesel engines equipped with diesel particulate filters (DPFs). The power-law fit reported in the figure corresponds to the Bare Quartz data (blue). The Artifact-corrected-fit (red dotted line) is modeled using Eq. S3b,a with $C_{OA} = 7.37 * EF_{OM}$.

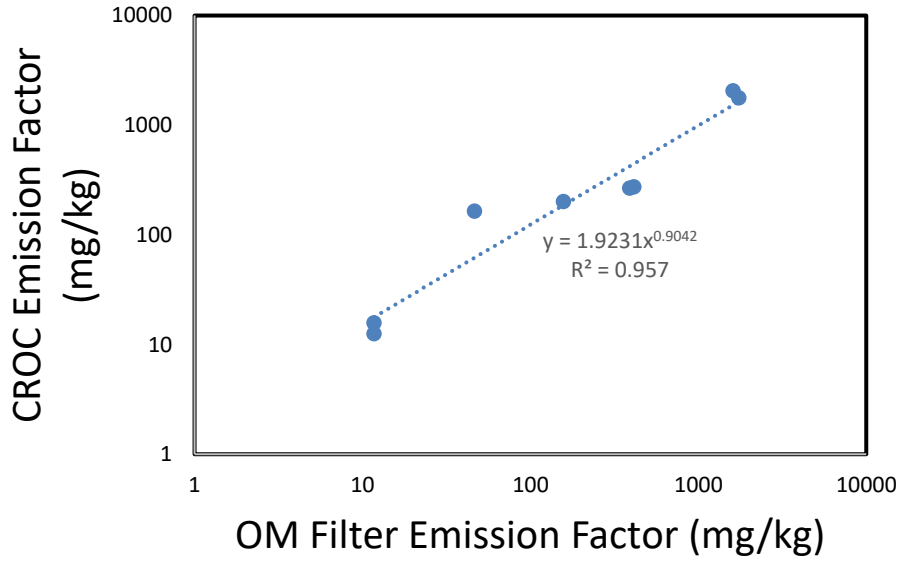

Figure S11. CROC emission factor as a function of filter-based OM emission factor for nonroad gasoline sources.

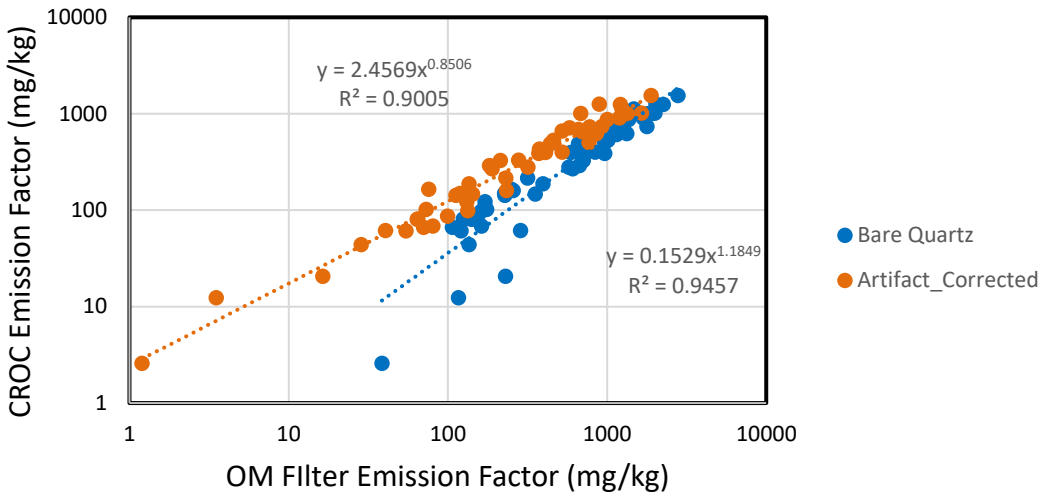

Figure S12. CROC emission factor as a function of filter-based OM emission factor for nonroad diesel non-DPF sources.

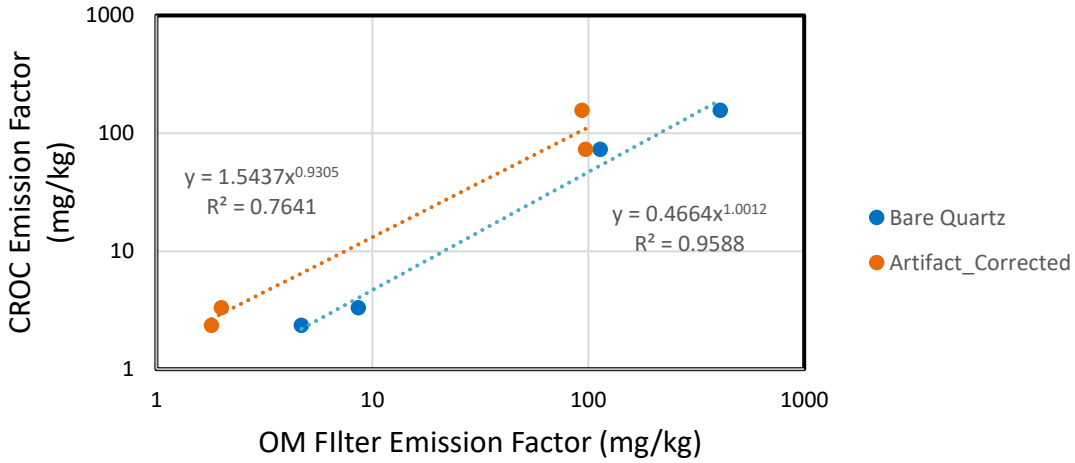

Figure S13. CROC emission factor as a function of filter-based OM emission factor for nonroad diesel DPF sources.

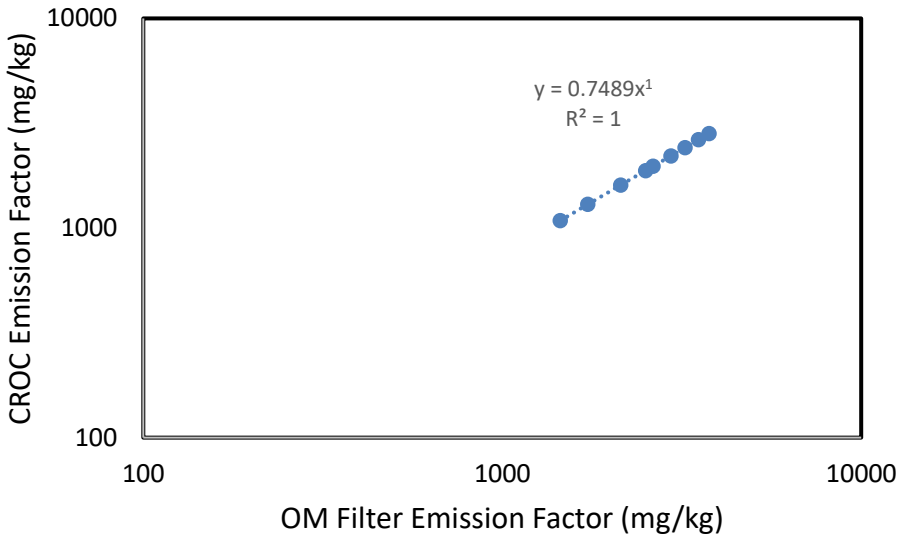

Figure S14. CROC emission factor as a function of filter-based OM emission factor for marine residual oil sources.

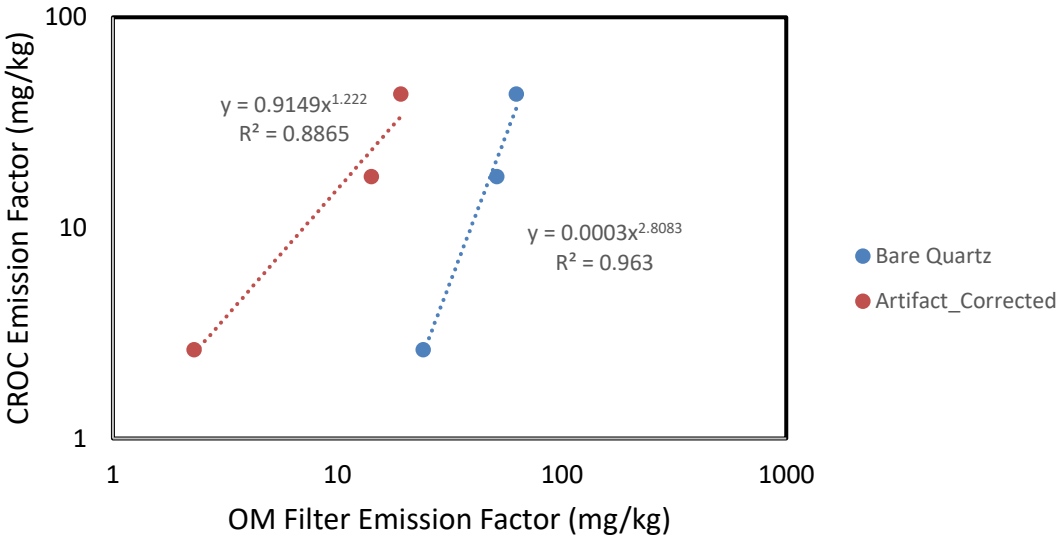

Figure S15. CROC emission factor as a function of filter-based OM emission factor for aircraft gas turbine sources.

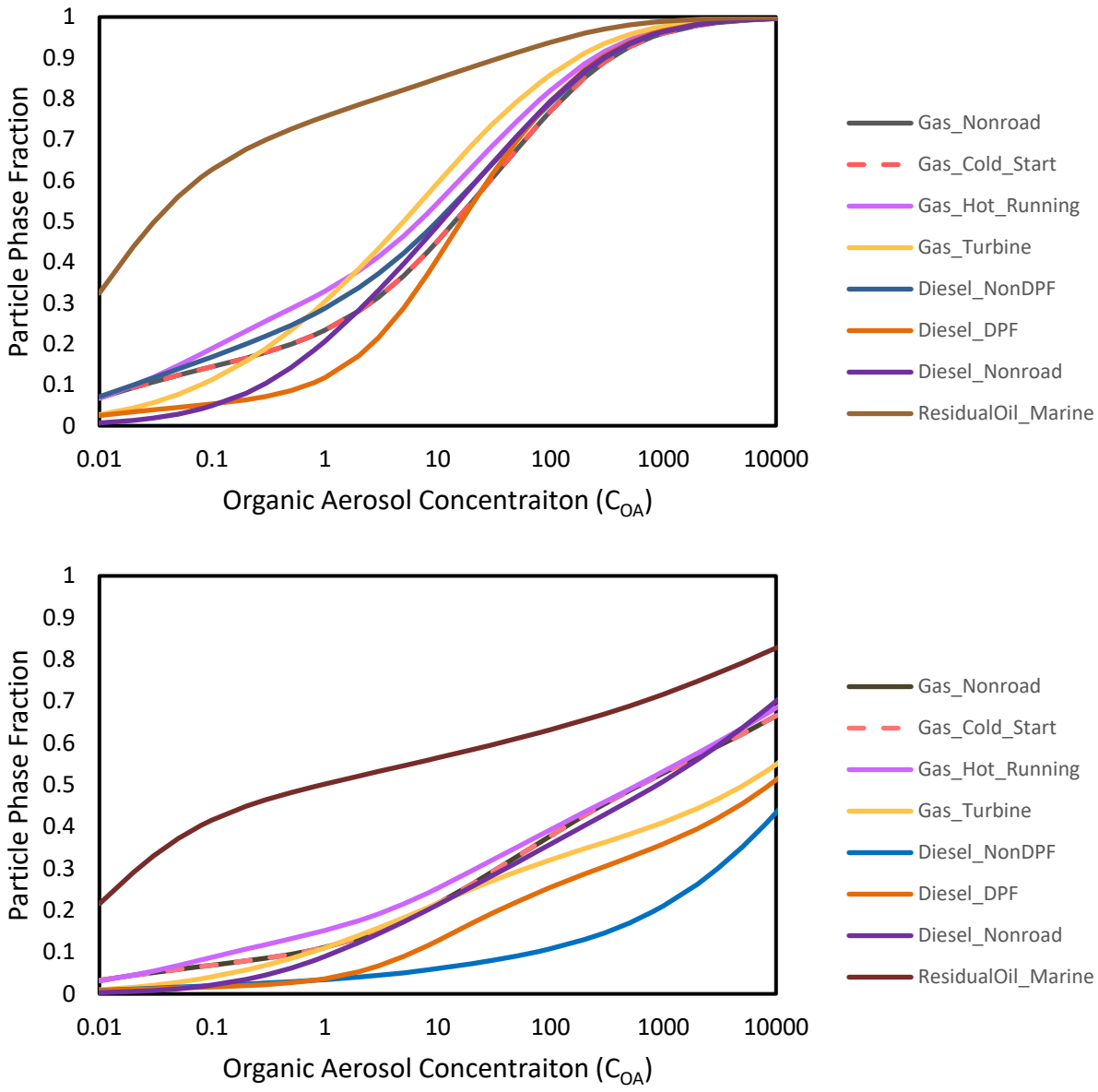

Figure S16. Partitioning behavior for mobile sector combustion sources at 298 K. (Top) Compounds span the range of CROC volatility, with $C^* < 320$ μg m^{-3}. (Bottom) Compounds include some IVOCs with volatility up to $C^* < 3.2 \times 10^5$ μg m^{-3}. Volatility parameters are provided in Table S6.

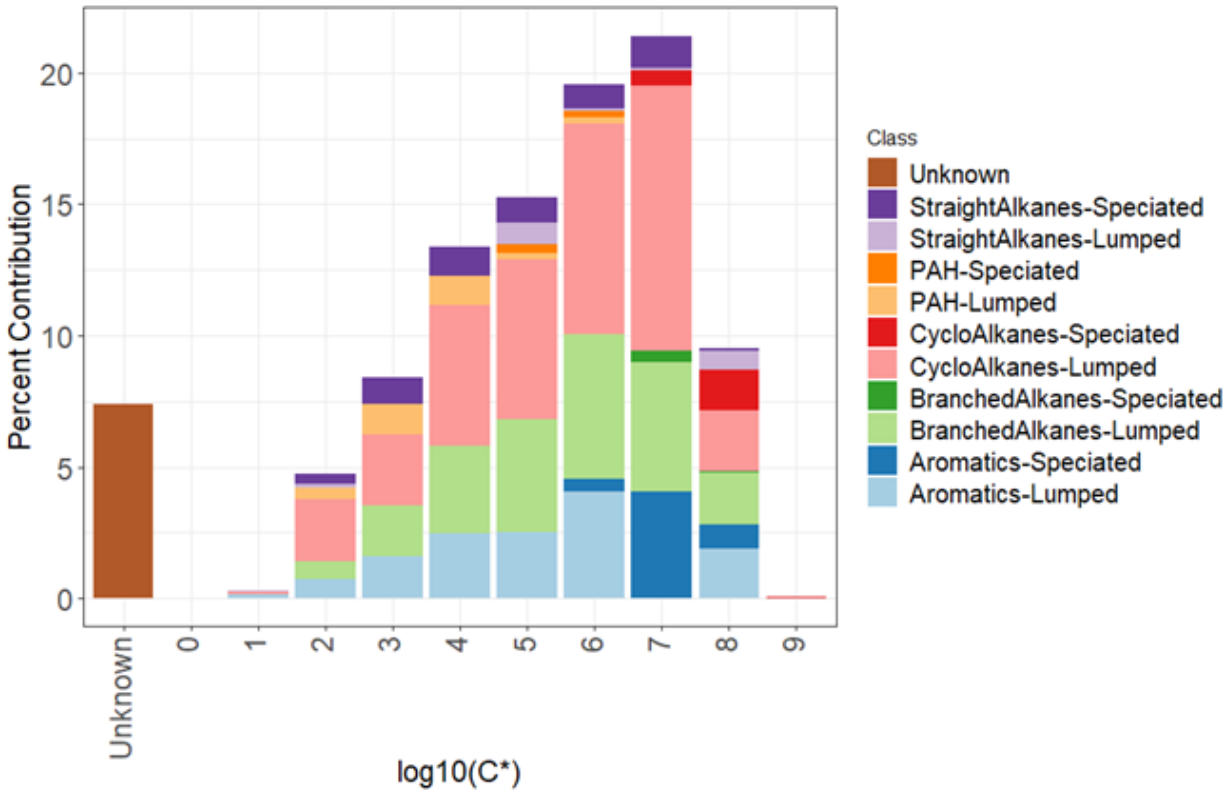

Figure S17. Volatility resolved liquid diesel – California Composite VOC speciation profile (profile number 95120c) created from Gentner et al.(Gentner et al., 2012) This profile contains the mass of the explicit species (speciated) and lumped species which are classified by functional group and saturation concentration, C*.

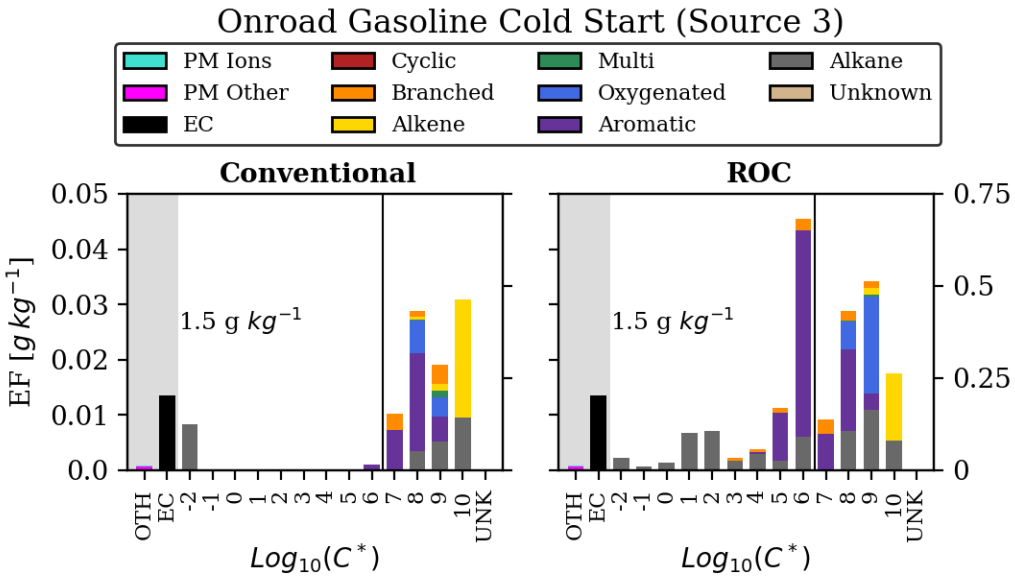

Figure S18. Emission factors for organic and non-organic components of PM and gases for Tier 2 onroad gasoline cold starts for the Conventional and ROC approaches. The gray shaded regions correspond to PM components not included in ROC emissions. ROC updates to this source are characterized by increases in the SVOC and IVOC range with little change to the total in the VOC range.

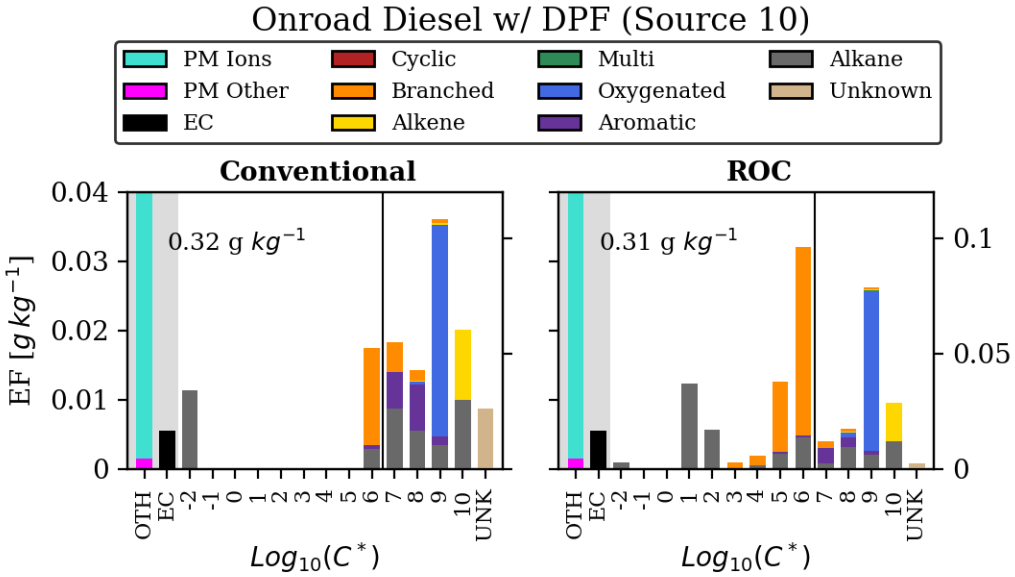

Figure S19. Emission factors for organic and non-organic components of PM and gases for onroad heavy duty diesel with particulate filters for the Conventional and ROC approaches. The gray shaded regions correspond to PM components not included in ROC emissions. These data are also plotted in Fig. 1. ROC updates to this source are characterized by increases in the SVOC and IVOC range and decreases to the $\log_{10}C^* = 10^{-2}$ species and decreases in the total across the VOC range.

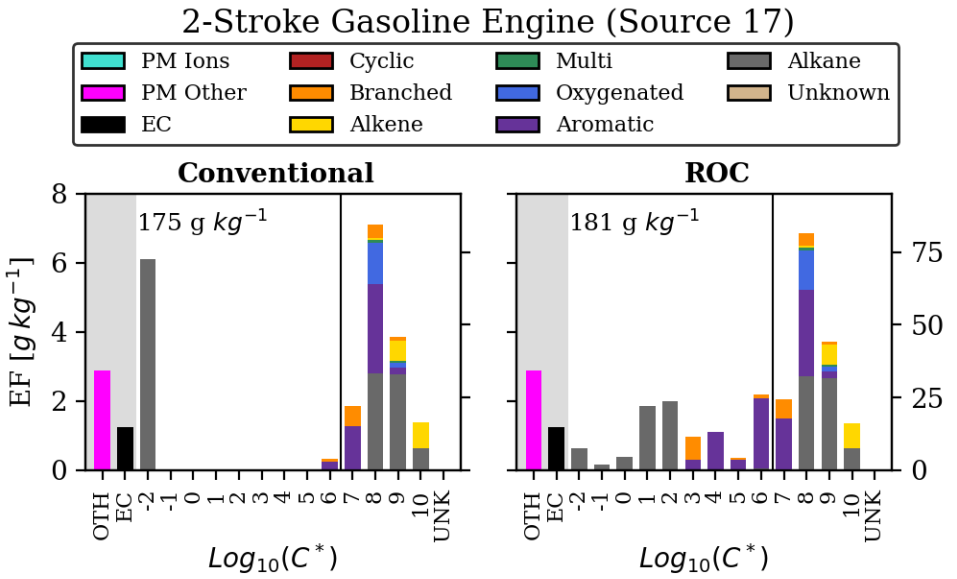

Figure S20. Emission factors for organic and non-organic components of PM and gases for nonroad 2-stroke gasoline engines for the Conventional and ROC approaches. The gray shaded regions correspond to PM components not included in ROC emissions. ROC updates to this source include increases in SVOC and IVOC, decrease to total CROC, and little change in the VOC range.

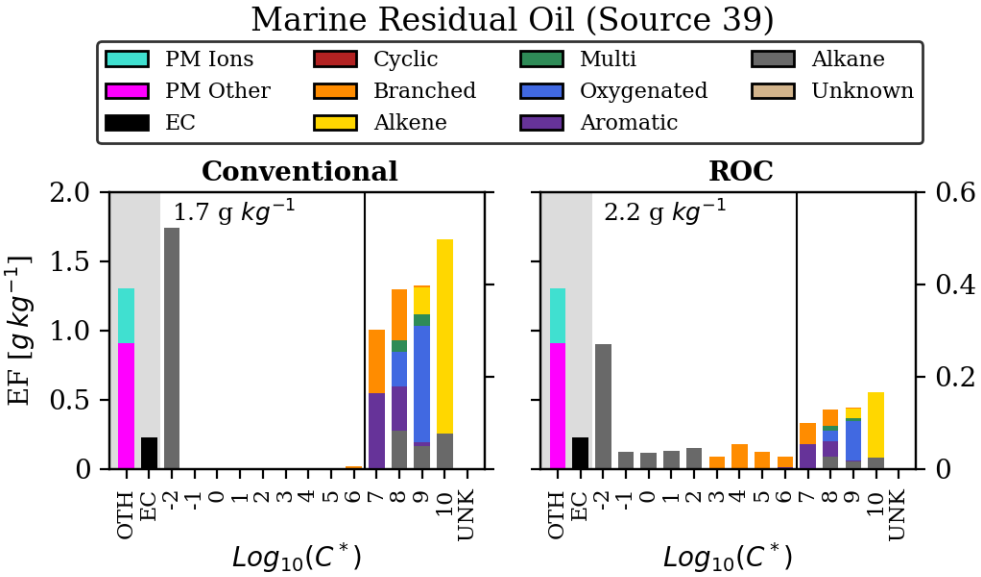

Figure S21. Emission factors for organic and non-organic components of PM and gases for marine residual oil-fueled sources for the Conventional and ROC approaches. The gray shaded regions correspond to PM components not included in ROC emissions. ROC updates to this source include increases to SVOCs and IVOCs, large remaining LVOC ($log_{10}C^* = 10^{-2}$), and substantially reduced total VOC.

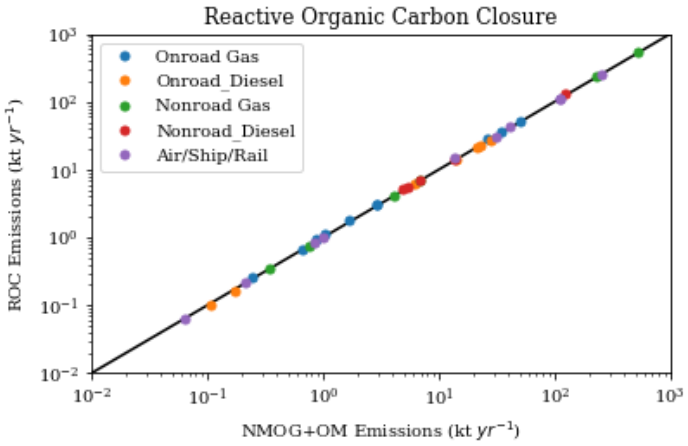

Figure S22. Correlation of annual OM filter plus NMOG emissions from conventional approach compared to annual ROC emissions using new GROC and CROC translation methods. Each point represents one source from Table S1a.

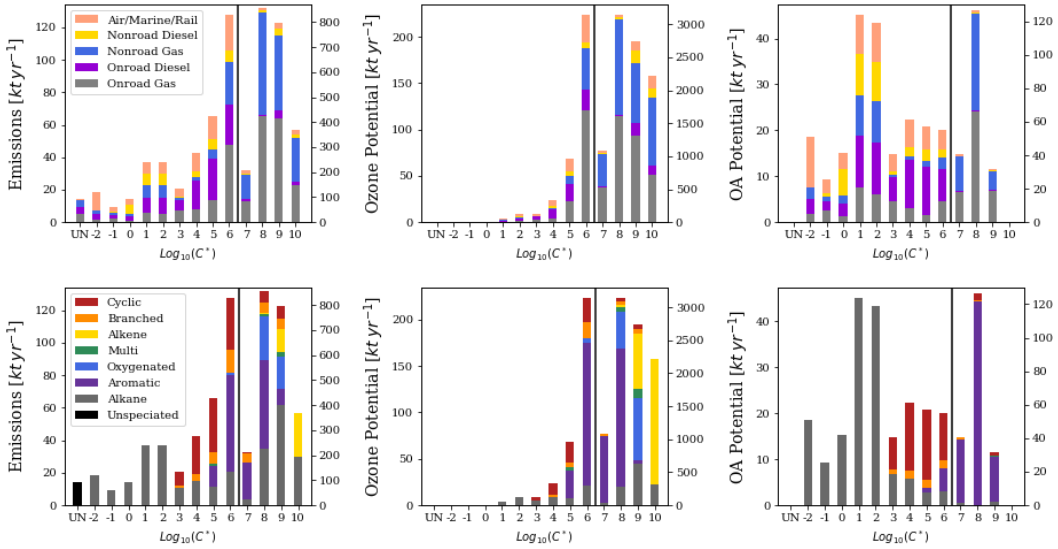

Figure S23. Mobile-source volatility-resolved ROC emissions, O_3 potential and OA potential, segregated by source sector (top row) and chemical functionality (bottom row).

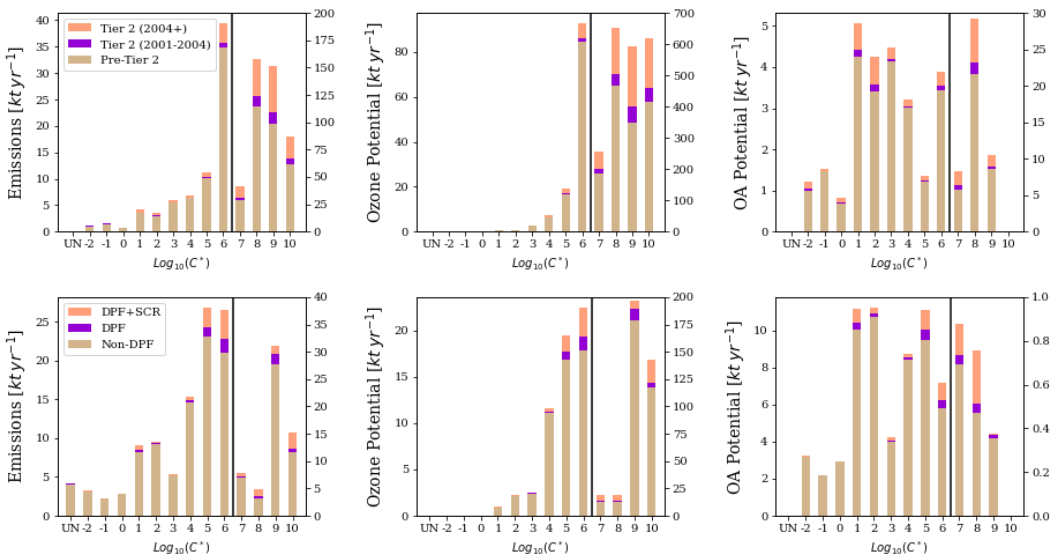

Figure S24. Onroad vehicle ROC emissions, O_3 potential, and OA potential distributed by volatility and emission control tier. The top row is presents light duty gasoline vehicle emissions for pre-Tier 2, the transition to Tier 2 from 2001-2004, and Tier 2 and newer from 2004 onward. The bottom row presents heavy duty diesel emissions for vehicles without diesel particulate filters (non-DPF), vehicles equipped with a DPF, and vehicles equipped with a DPF and a Selective Catalytic Reduction (SCR) system.

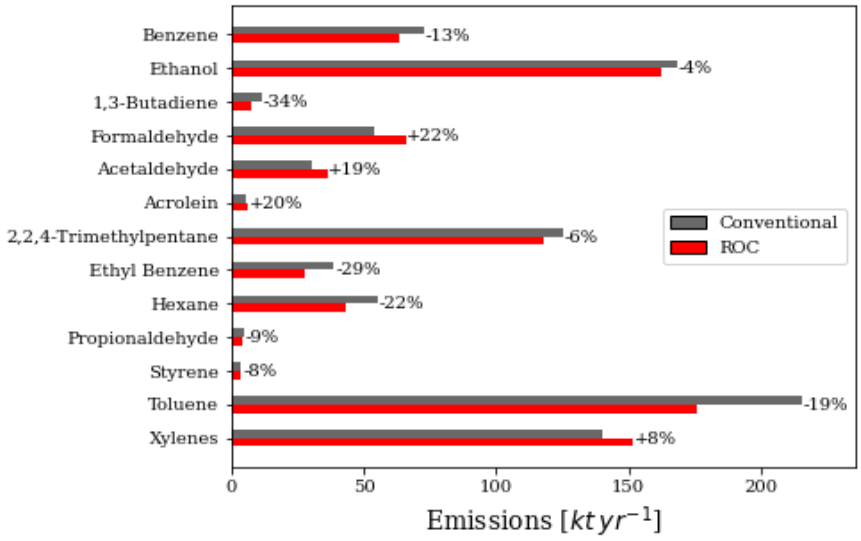

Figure S25. Changes to annual total MOVES emissions using the ROC approach (this study) for integrated species, a subset of the U. S. EPA hazardous air pollutant (HAP) list.

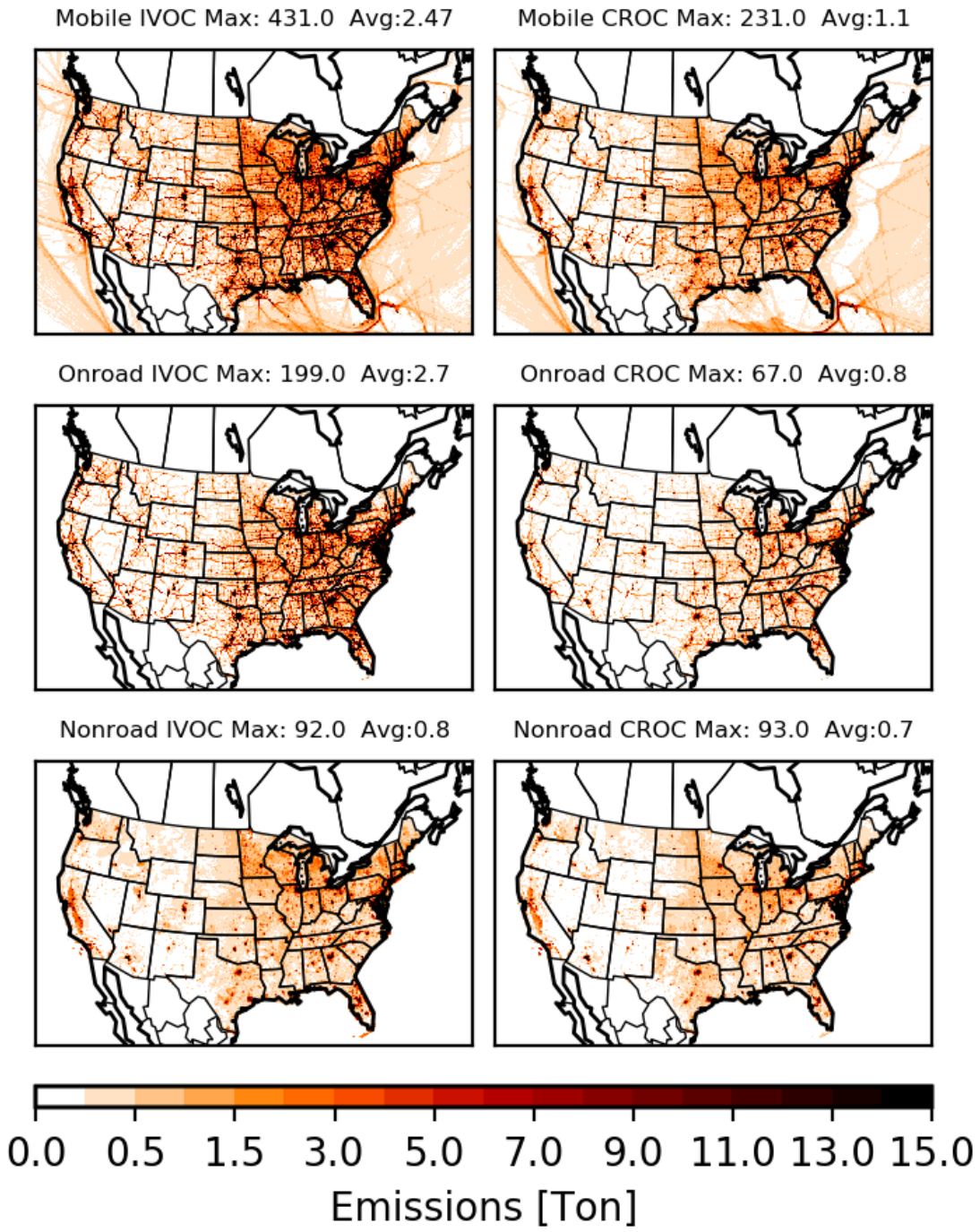

Figure S26. Spatial distribution of annual total IVOC and CROC emissions (in tons yr^{-1}). The average emission rate shown in the subtitles of each panel are population-weighted.

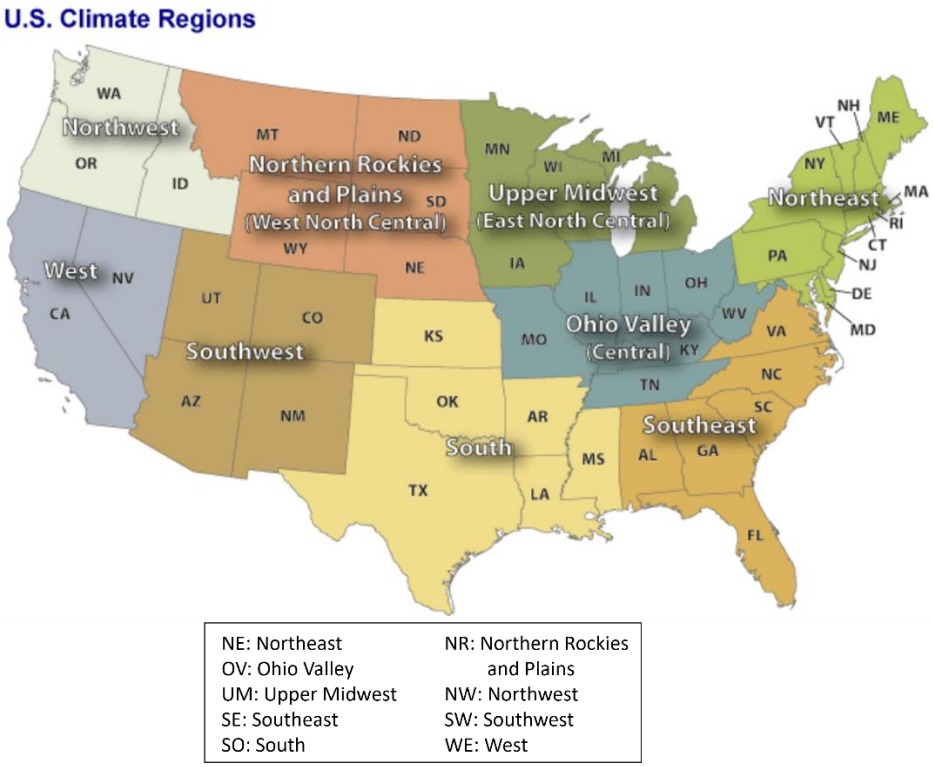

Figure S27. Map of the NOAA U.S. climate regions. Image source: https://www.ncdc.noaa.gov/monitoring-references/maps/us-climate-regions.php

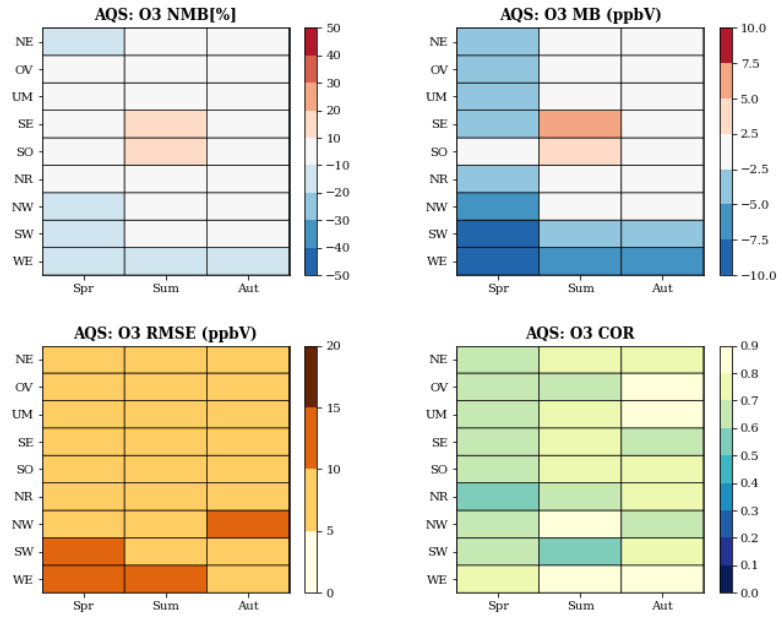

Figure S28. Statistical evaluation of CMAQ O_3 predictions with data from the Air Quality System network during 2017. Data are selected for the seasons with significant ozone formation. Results are shown for the CMAQ_ROC simulation. Each row corresponds to a U.S. geographical region identified by the abbreviation to the left and defined in Fig. S27.

a.

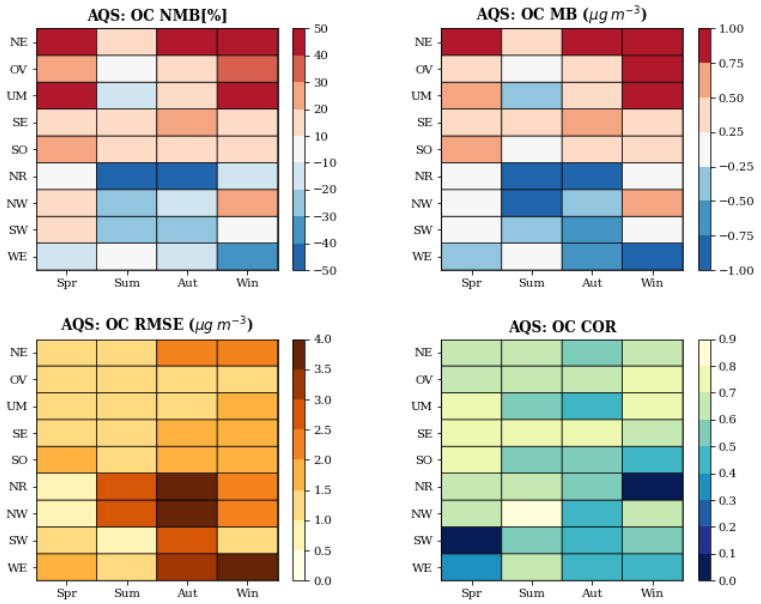

b.

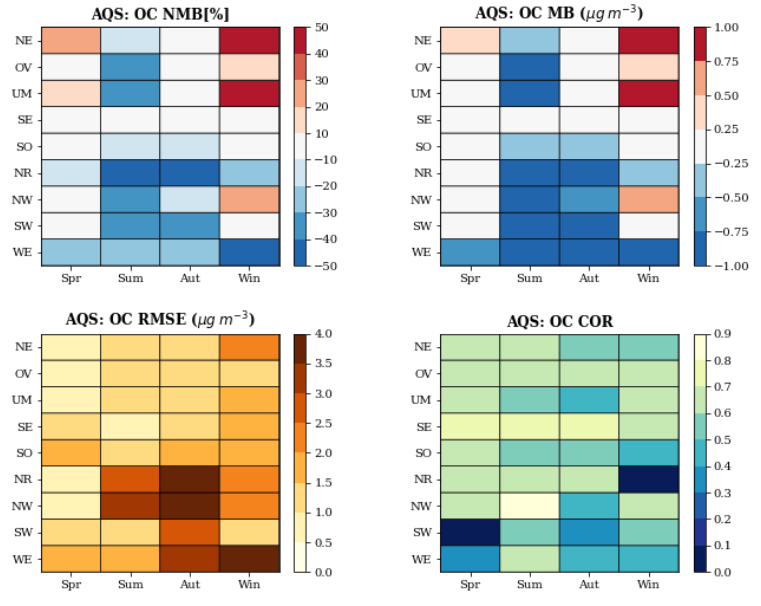

Figure S29. Statistical evaluation of CMAQ organic carbon (OC) predictions with data from the Air Quality System network during 2017 for the EQUATES (a) and CMAQ_ROC (b) simulations. Each row corresponds to a U.S. geographical region identified by the abbreviation to the left and defined in Fig. S27.

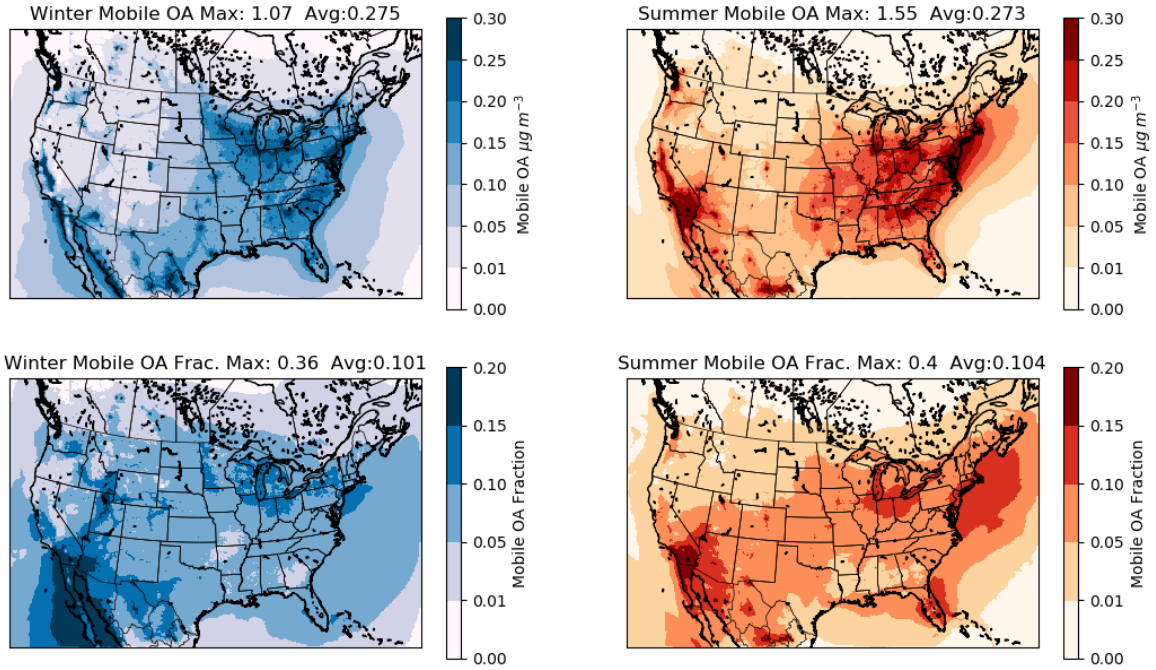

Figure S30. Spatial distribution of total organic aerosol concentrations (top row) attributable to mobile sources and fraction of mobile source OA to the total concentration from all sources (bottom row) in the winter (left) and summer (right) of 2017. The 'Avg' metric is the population-weighted average.

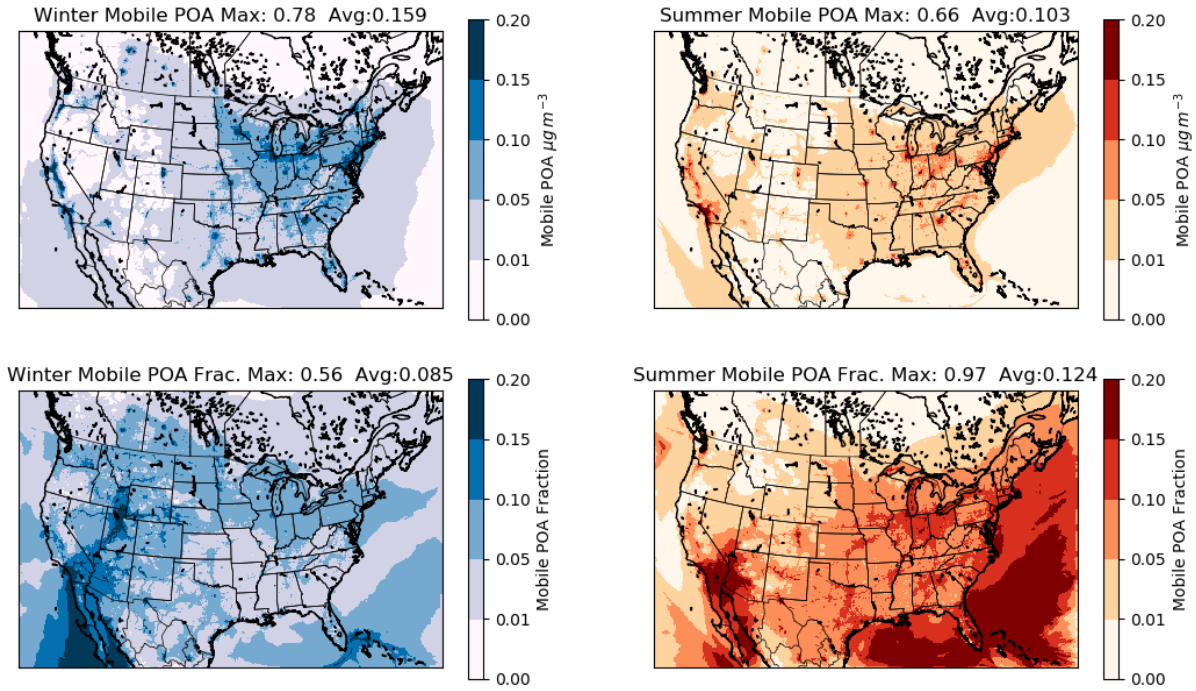

Figure S31. Spatial distribution of total primary organic aerosol (POA) concentrations (top row) attributable to mobile sources and fraction of mobile source POA to the total concentration from all sources (bottom row) in the winter (left) and summer (right) of 2017. The 'Avg' metric is the population-weighted average.

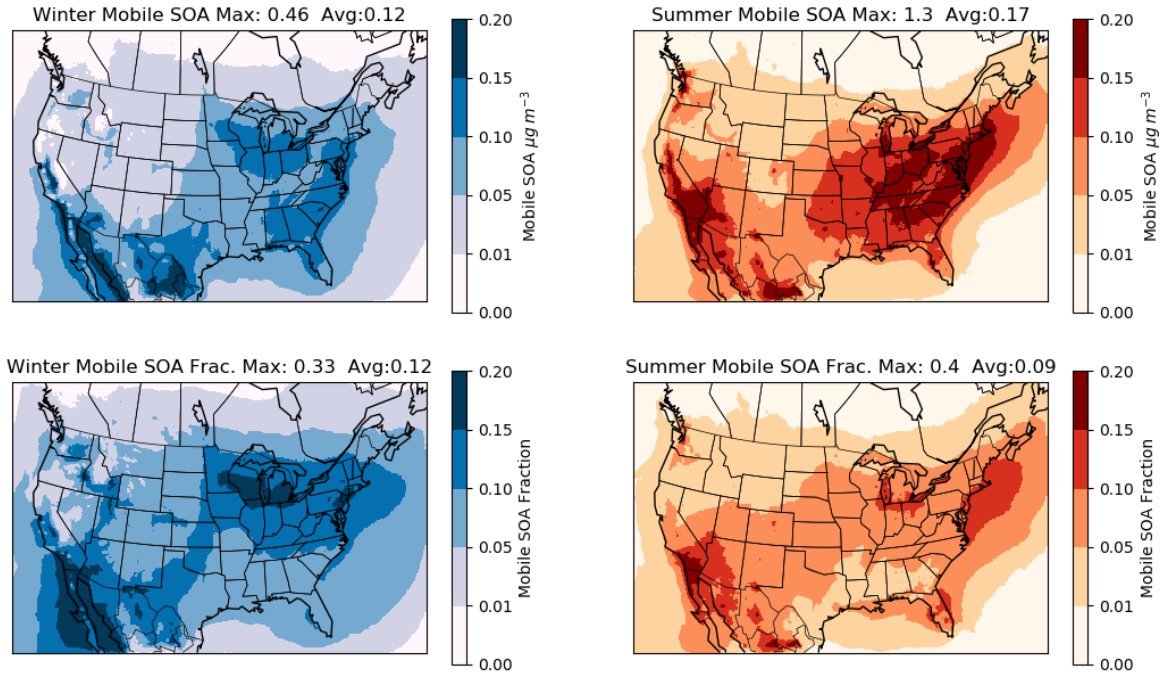

Figure S32. Spatial distribution of total secondary organic aerosol (SOA) concentrations (top row) attributable to mobile sources and fraction of mobile source SOA to the total concentration from all sources (bottom row) in the winter (left) and summer (right) of 2017. The 'Avg' metric is the population-weighted average.

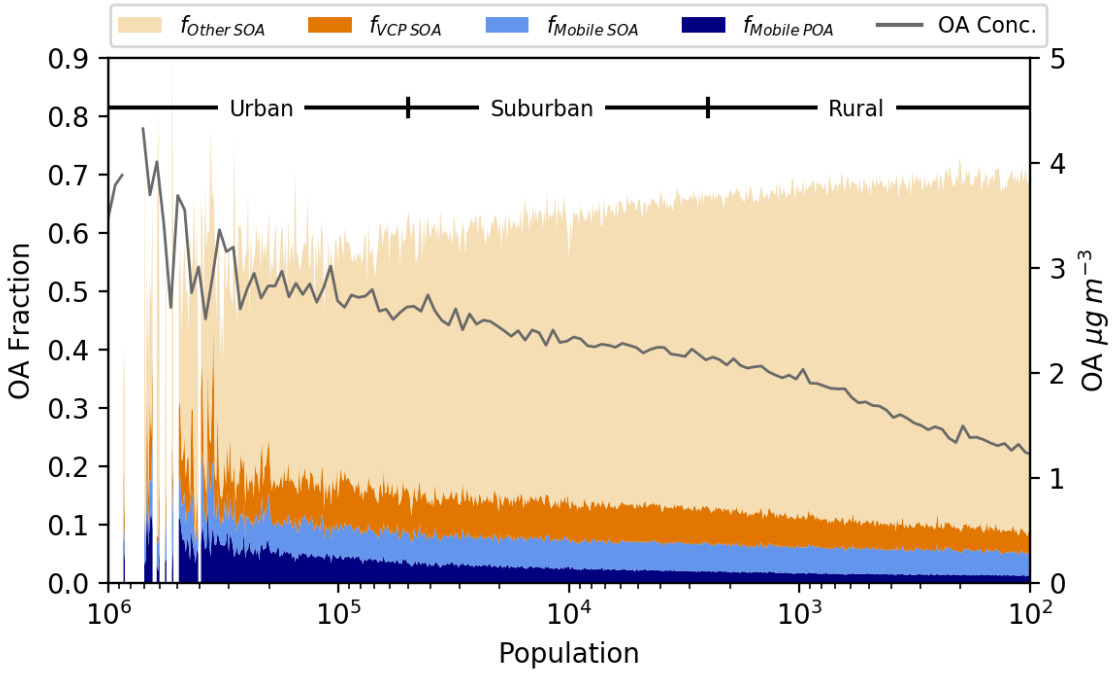

Figure S33. Histogram of annual-average OA fractional contributions (stacked trends, left axis) from mobile POA, mobile SOA, VCP SOA, and other SOA (including biogenic and anthropogenic sources) as a function of the human population of the corresponding CMAQ grid cell. Also shown is the total OA concentration in the gray line (right axis).

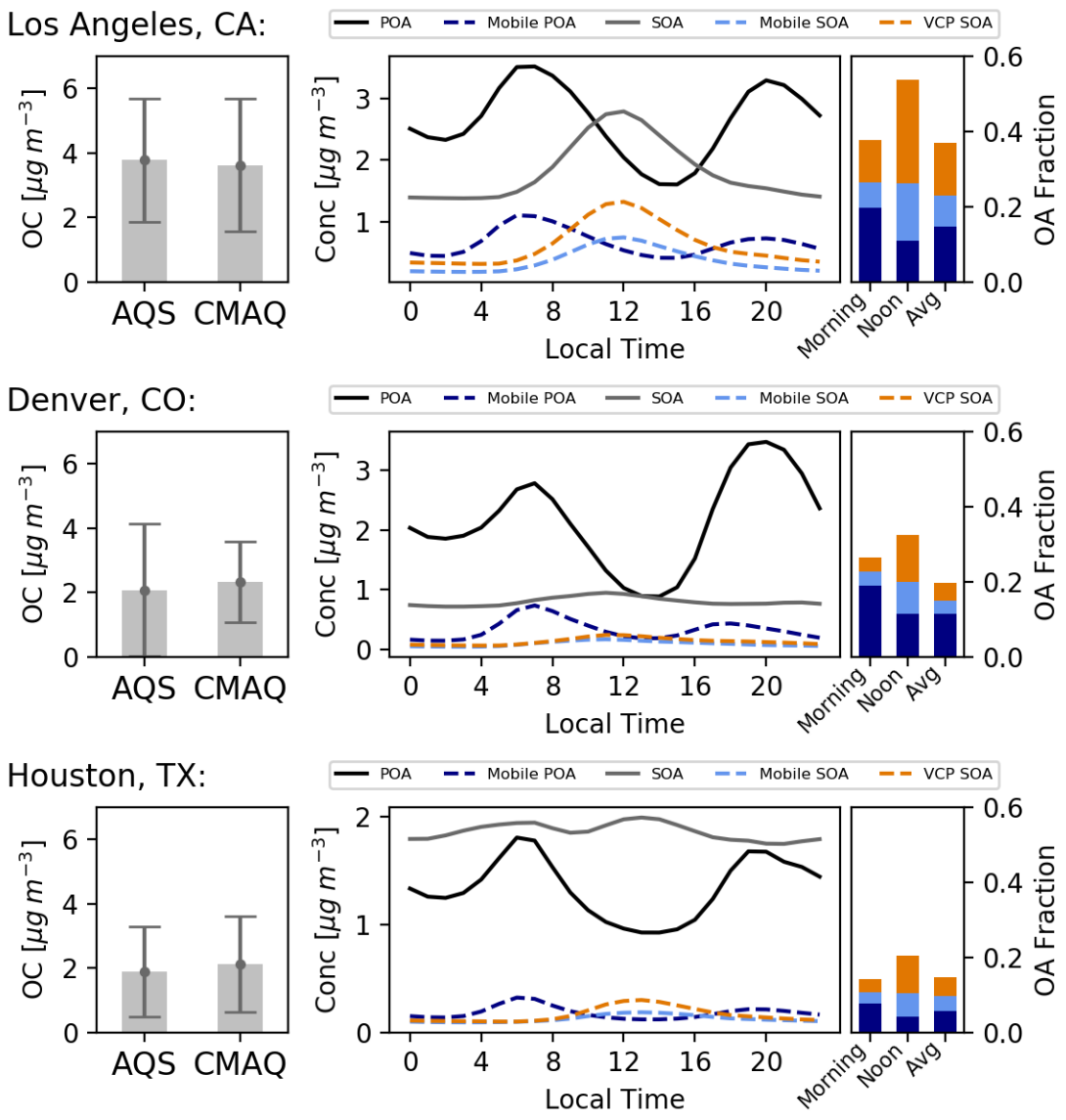

Figure S34. (left) Annual average organic carbon (OC) concentration measured at Air Quality System sites and predicted by CMAQ with updated mobile ROC emissions for select cities in the west and central U.S. during 2017. (center) Annual diurnal average concentrations of total POA and SOA, mobile source POA and SOA, and VCP SOA at the corresponding city predicted by CMAQ. (right) Model-predicted fractional contributions from mobile and VCP sources to total OA for the morning (6 – 9 am local time), at noon, and averaged for the day.

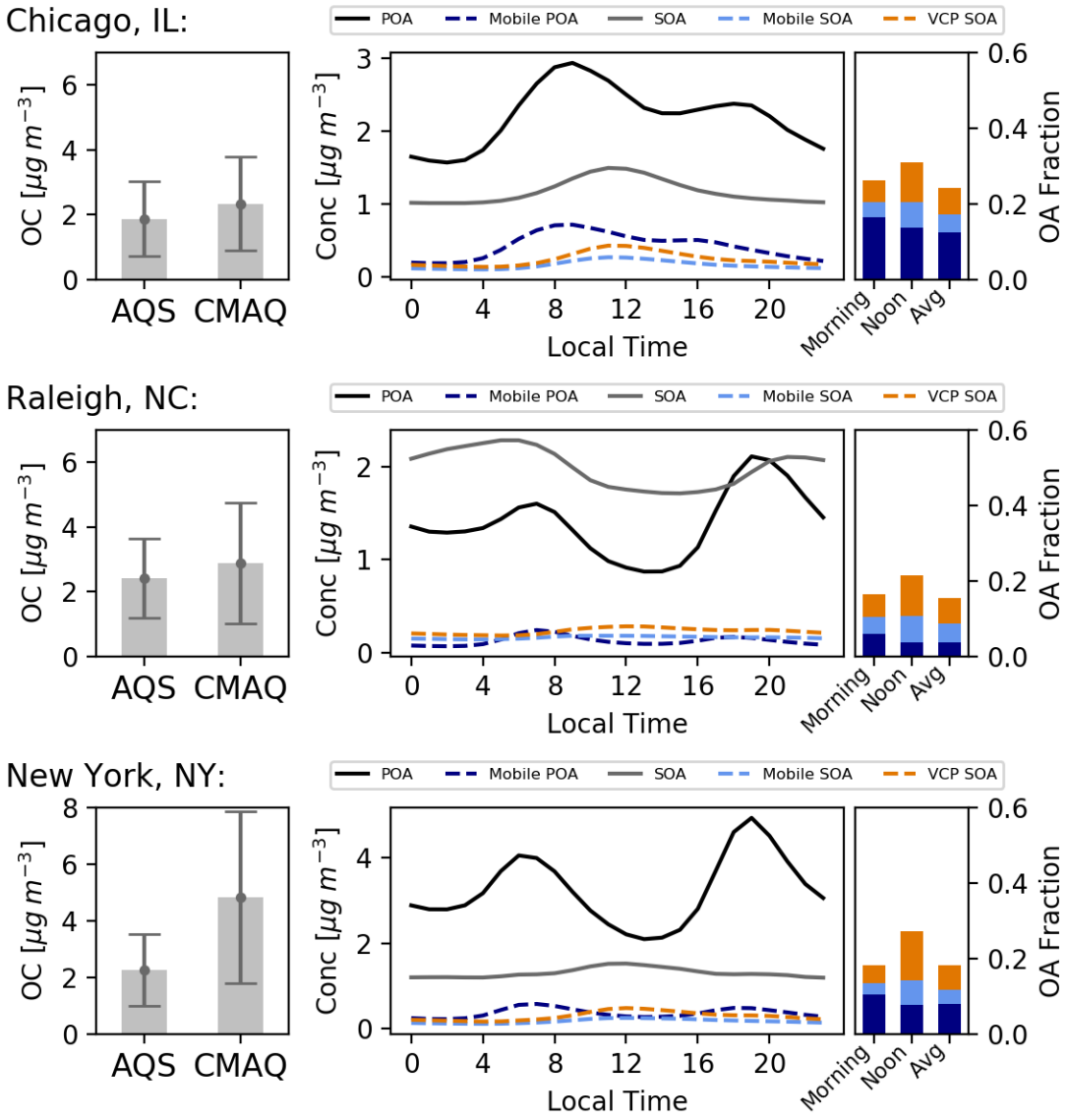

Figure S35. As in Fig. S34 for three select cities in the Eastern U.S.

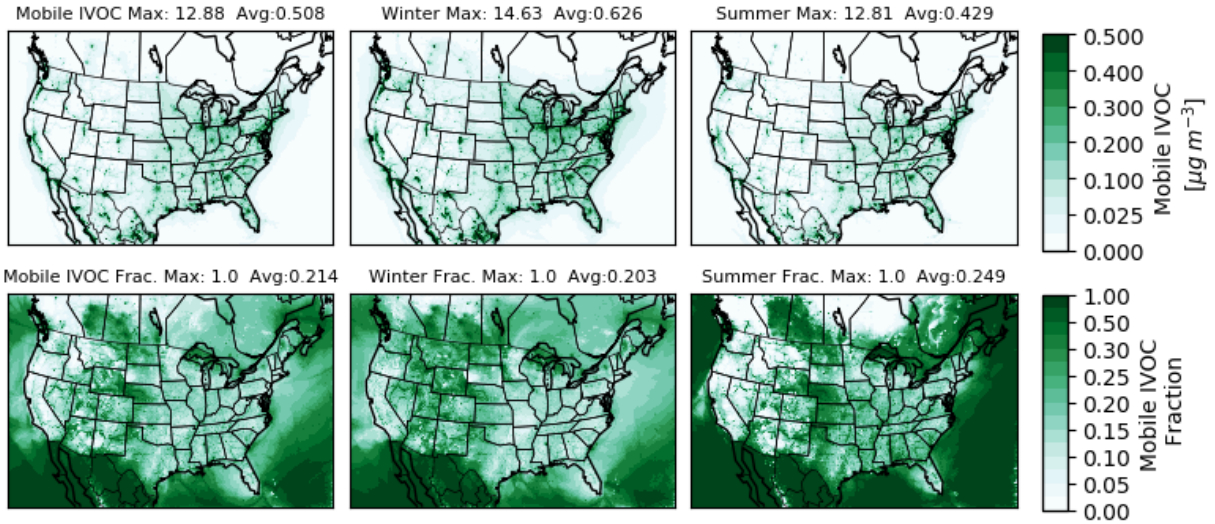

Figure S36. Spatial distribution of IVOC concentrations (top row) attributable to mobile sources and fraction of mobile source IVOC to the total concentration from all sources (bottom row) in the winter (left) and summer (right) of 2017. The 'Avg' metric is the population-weighted average.

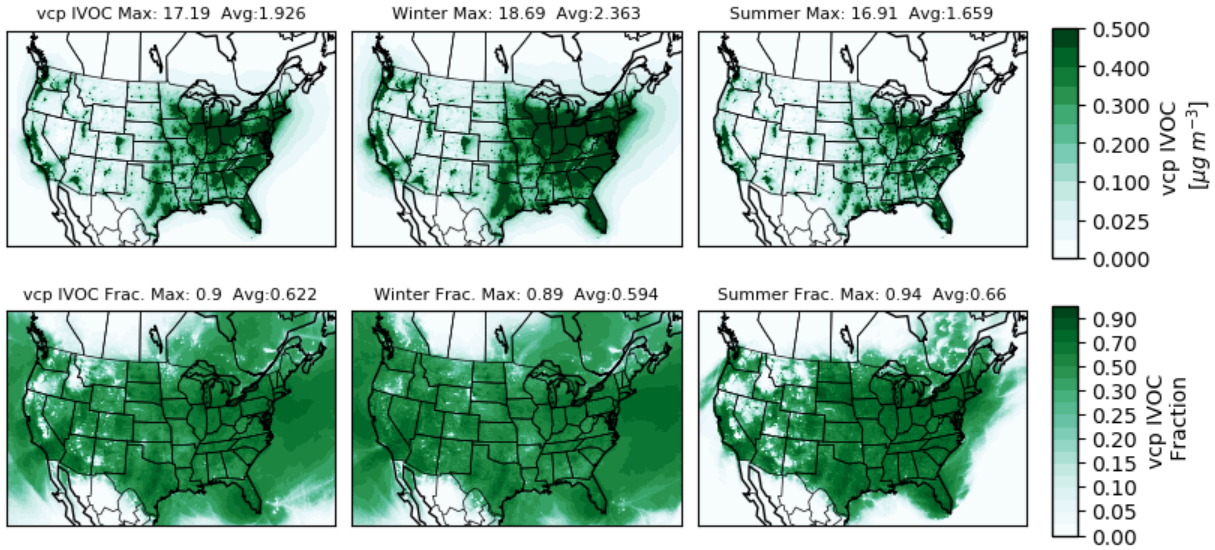

Figure S37. Spatial distribution of IVOC concentrations (top row) attributable to VCP sources and fraction of VCP source IVOC to the total concentration from all sources (bottom row) in the winter (left) and summer (right) of 2017. The 'Avg' metric is the population-weighted average.

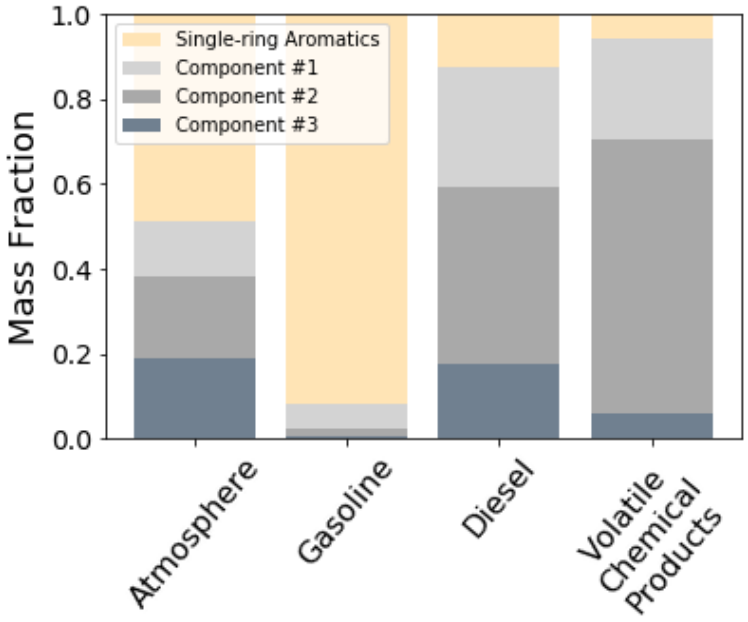

Figure S38. Single-ring aromatic and IVOC contributions to CMAQ-predicted IVOCs (Atmosphere) and emissions inputs used for Pasadena, CA during 2017. IVOC components 1, 2, and 3 are comprised of IVOCs with the following C^* values (in μg m^{-3}): Component 1 includes 10^6; Component 2 includes 10^5 and 10^4, Component 3 includes 10^3. The 'Atmosphere' predictions are back-projected to 2010 for comparison to CalNex observations.

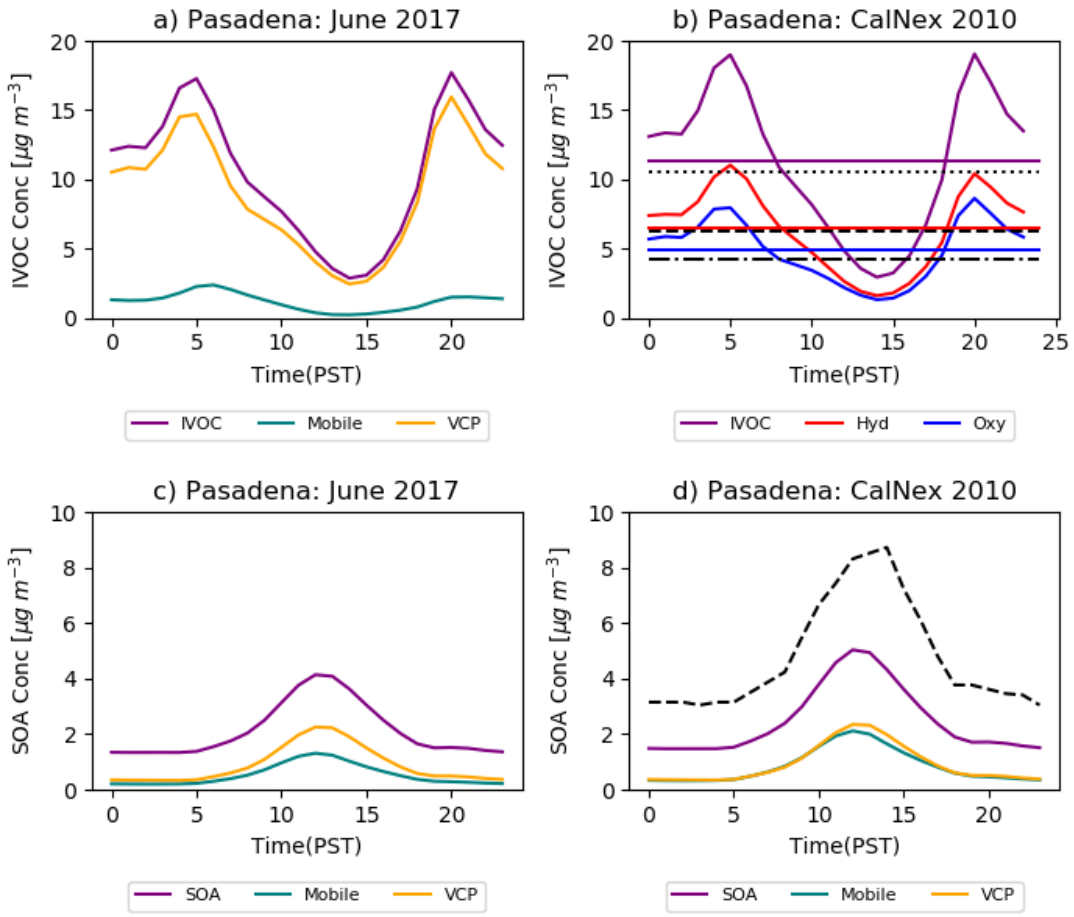

Figure S39. Average diurnally averaged IVOC concentration predictions for Pasadena, California in June 2017 (left) and back-projected to the CalNex measurement campaign in June 2010. The left panel includes IVOCs attributable to Mobile (green) and VCP (orange) sources. The right panel includes hydrocarbon (red) and oxygenated (blue) contributions to IVOCs. The dotted, dashed, and dotted-dashed lines in panel b correspond to the CalNex campaign average concentrations of total IVOC, hydrocarbon IVOC, and oxygenated IVOC, respectively, with the model averages shown in solid lines.(Zhao et al., 2014) The dashed line in panel d corresponds to total oxygenated OA concentrations observed during CalNex.

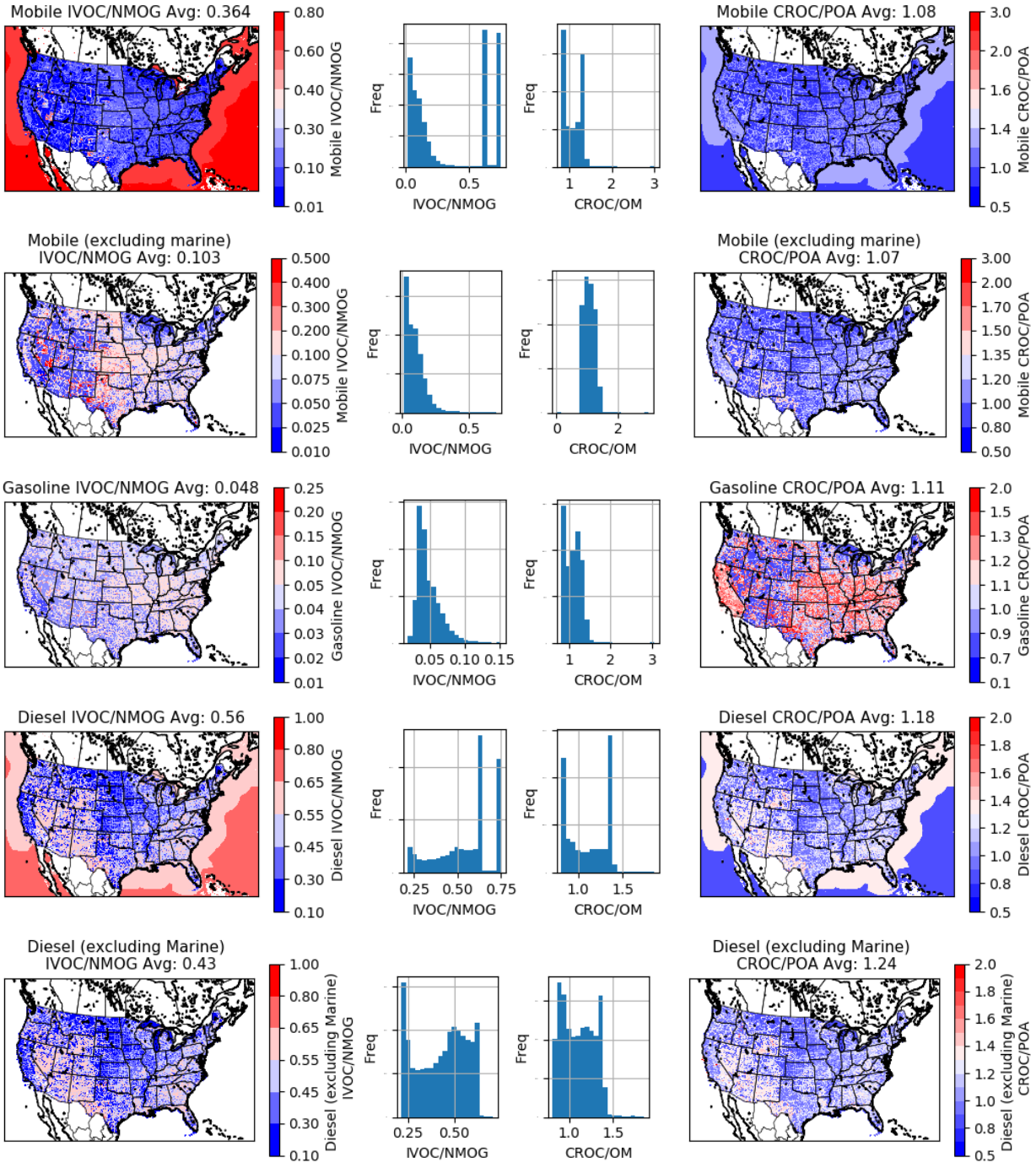

Figure S40. Spatial distribution and histograms of IVOC/NMOG (left) and CROC/POA (right) for select levels of aggregations of mobile sources for the 2017 simulation year. The first row corresponds to all mobile sources, the second row to mobile sources excluding marine vessels, the third row to gasoline sources, and the fourth row to diesel sources including marine vessels.